Tissue Engineering

© Mary Ann Liebert, Inc.

DOI: 10.1089/ten.TEA.2019.0204

Multi-Material Dual Gradient 3D Printing for Osteogenic Differentiation and Spatial Segregation

Brandon T. Smith, BS,[1-4,†] Sean M. Bittner, BS,[1-3,†] Emma Watson, BS,[1-4] Mollie M. Smoak, BS,[1-3] Luis Diaz-Gomez, PhD,[1-3] Eric R. Molina, BS,[1-4] Yu Seon Kim, BS,[1-3] Carrigan D. Hudgins[1-3], Anthony J. Melchiorri, PhD,[1-3] David W. Scott, PhD,[5] K. Jane Grande-Allen, PhD,[1] James J. Yoo, MD, PhD,[3,6] Anthony Atala, MD,[3,6] John P. Fisher, PhD,[3,7] and Antonios G. Mikos, PhD[1-3*]

[1]Department of Bioengineering, Rice University, Houston, TX 77030, USA;

[2]Biomaterials Lab, Rice University, Houston, TX 77030, USA;

[3]NIH / NIBIB Center for Engineering Complex Tissues, USA;

[4]Medical Scientist Training Program, Baylor College of Medicine, Houston, TX, USA;

[5]Department of Statistics, Rice University, Houston, TX 77030, USA;

[6]Wake Forest Institute for Regenerative Medicine, Winston-Salem, NC 27101, USA

[7]Fischell Department of Bioengineering, University of Maryland, College Park, MD, USA.

†These authors contributed equally to the work

*To whom correspondence may be addressed:

Antonios G. Mikos, PhD

Department of Bioengineering, MS-142

BioScience Research Collaborative

Rice University

6500 Main Street

Houston, TX-77030

E-mail: mikos@rice.edu

Downloaded by Ucsf Library University of California San Francisco from www.liebertpub.com at 11/08/19. For personal use only.

Tissue Engineering
Multi-Material Dual Gradient 3D Printing for Osteogenic Differentiation and Spatial Segregation (DOI: 10.1089/ten.TEA.2019.0204)
This paper has been peer-reviewed and accepted for publication, but has yet to undergo copyediting and proof correction. The final published version may differ from this proof.

Tel: (713) 348-5355

Fax: (713) 348-4244

Downloaded by Ucsf Library University of California San Francisco from www.liebertpub.com at 11/08/19. For personal use only.

Tissue Engineering
Multi-Material Dual Gradient 3D Printing for Osteogenic Differentiation and Spatial Segregation (DOI: 10.1089/ten.TEA.2019.0204)
This paper has been peer-reviewed and accepted for publication, but has yet to undergo copyediting and proof correction. The final published version may differ from this proof.

Abstract

In this study of 3D printed composite β-tricalcium phosphate (β-TCP)/hydroxyapatite (HA)/poly(ε-caprolactone) (PCL)-based constructs, the effects of vertical compositional ceramic gradients and architectural porosity gradients on the osteogenic differentiation of rabbit bone marrow derived mesenchymal stem cells (MSCs) were investigated. Specifically, three different concentrations of β-TCP (0, 10, and 20 wt%) and three different porosities (33 ± 4 %, 50 ± 4 %, and 65 ± 3 %) were examined to elucidate the contributions of chemical and physical gradients on the biochemical behavior of MSCs and the mineralized matrix production within a 3D culture system. By delaminating the constructs at the gradient transition point, the spatial separation of cellular phenotypes could be specifically evaluated for each construct section. Results indicated that increased concentrations of β-TCP resulted in up-regulation of osteogenic markers including alkaline phosphatase activity and mineralized matrix development. Furthermore, MSCs located within regions of higher porosity displayed a more mature osteogenic phenotype compared to MSCs in lower porosity regions. These results demonstrate that 3D printing can be leveraged to create multiphasic gradient constructs to precisely direct the development and function of MSCs, leading to a phenotypic gradient.

Downloaded by Ucsf Library University of California San Francisco from www.liebertpub.com at 11/08/19. For personal use only.

Tissue Engineering
Multi-Material Dual Gradient 3D Printing for Osteogenic Differentiation and Spatial Segregation (DOI: 10.1089/ten.TEA.2019.0204)
This paper has been peer-reviewed and accepted for publication, but has yet to undergo copyediting and proof correction. The final published version may differ from this proof.

Impact Statement:

In the present study, 3D printed ceramic/polymeric constructs containing discrete vertical gradients of both composition and porosity were fabricated to precisely control the osteogenic differentiation of mesenchymal stem cells. By making simple alterations in construct architecture and composition, constructs containing heterogenous populations of cells were generated, where gradients in scaffold design led to corresponding gradients in cellular phenotype. The study demonstrates that 3D printed multiphasic composite constructs can be leveraged in order to create complex heterogeneous tissues and interfaces.

Keywords: Gradients, osteogenic differentiation, multiphasic scaffold, bone tissue engineering, construct

Downloaded by Ucsf Library University of California San Francisco from www.liebertpub.com at 11/08/19. For personal use only.

Tissue Engineering
Multi-Material Dual Gradient 3D Printing for Osteogenic Differentiation and Spatial Segregation (DOI: 10.1089/ten.TEA.2019.0204)
This paper has been peer-reviewed and accepted for publication, but has yet to undergo copyediting and proof correction. The final published version may differ from this proof.

Downloaded by Ucsf Library University of California San Francisco from www.liebertpub.com at 11/08/19. For personal use only.

Tissue Engineering
Multi-Material Dual Gradient 3D Printing for Osteogenic Differentiation and Spatial Segregation (DOI: 10.1089/ten.TEA.2019.0204)
This paper has been peer-reviewed and accepted for publication, but has yet to undergo copyediting and proof correction. The final published version may differ from this proof.

1. Introduction

In clinical practice, autogenous bone grafts are the gold standard for the treatment of bone defects, delayed unions, and non-unions (1). However, due to drawbacks associated with these grafts, such as donor site morbidity, surgical site pain, limited availability, and failure to adequately address the soft tissue-to-bone interface, research into future treatment methods increasingly focuses on the substantial advancement of constructs for tissue engineering (2-4). Native bone tissue has a complex heterogenous architecture that possesses regional differences in structure and composition (5). For example, cortical bone has a higher degree of mineralization and a 20-30% higher tissue compressive strength compared to trabecular bone (6-8). Additionally, long bones have a radial gradient in porosity when transitioning from trabecular to cortical bone (9). Cortical bone has an average porosity of 10-20%, while for trabecular bone the porosity ranges between 50-90% (10). Furthermore, defects of soft tissue-to-bone interfaces, such as the osteochondral unit, demonstrate an even more heterogenous structure because they are composed of relatively simple building blocks that combine to form exceedingly complex structures (11). With the advent of a diverse array of biofabrication techniques, one can now fabricate multiphasic constructs that recreate the complex architectural and compositional gradients present in tissues and interfaces (12).

To better recapitulate the complex heterogenous structure of tissue interfaces, several different techniques have been investigated that aim to restore the native zonal architecture and cellular phenotypic transitions. One such approach takes inspiration from nature, where different biological processes, such as wound healing, nerve regeneration, immune response, angiogenesis, and tissue architecture, are mediated by bioactive molecule gradients (13, 14). In this type of approach, the spatiotemporal patterning and dispersion of bioactive molecules such as growth factors is specifically controlled to create gradients in biochemical signaling, leading to the formation of heterogeneous tissues (15-18). As an example, the delivery of transforming growth factor-β1 (TGF-β1) and bone morphogenetic protein-2 (BMP-2) was leveraged in a graded manner to control the arrangement of regenerated cartilage and subchondral bone tissue (17). Another creative approach has leveraged modified

Downloaded by Ucsf Library University of California San Francisco from www.liebertpub.com at 11/08/19. For personal use only.

Tissue Engineering
Multi-Material Dual Gradient 3D Printing for Osteogenic Differentiation and Spatial Segregation (DOI: 10.1089/ten.TEA.2019.0204)
This paper has been peer-reviewed and accepted for publication, but has yet to undergo copyediting and proof correction. The final published version may differ from this proof.

viral vectors rather than growth factors to accomplish spatially-stratified phenotypic changes in cultured cells (19-21). Such demonstrations display the utility of viral vectors for therapeutic benefit. For example, the zonal organization of the soft tissue-to-bone interface can be recapitulated by seeding fibroblasts onto polymeric constructs that contained a graded distribution of a retroviral vector for transcription factor *Runx2* (21). However, both of these approaches leverage exogenous biologics or viral vectors to ultimately control the zonal organization, whereas it may be desirable to exclude these added factors.

One can additionally leverage 3D synthetic constructs for tissue engineering without relying on viral vectors or biologics and still impart a variety of mechanical and biochemical stimuli to affect cell behavior and phenotype. With respect to the physical attributes of the scaffold or environment, several studies have demonstrated that, in particular, porosity and pore size have significant implications on the osteogenic differentiation of mesenchymal stem cells (MSCs) (22-26). *In vitro* it was demonstrated that a construct's mean pore size affects the cellular activity of cultured pre-osteogenic cells, and that small changes in the mean pore size can dramatically change cell adhesion and distribution, thereby affecting the osteogenic differentiation by impacting the paracrine signaling distance (27, 28). Many cytocompatible synthetic polymers exhibit a bioinert surface resulting in minimal tissue response or capability for direct cell interaction without the assistance of additives or adsorbed proteins (29, 30). By incorporating additives within synthetic polymers, such as poly(ε-caprolactone) (PCL), one can improve the attachment, proliferation, and ultimately affect the osteogenesis of MSCs (31-38). Among other such additives, ceramic materials, such as hydroxyapatite (HA) and β-tricalcium phosphate (β-TCP), are widely used as synthetic bone substitutes that have been shown to affect the osteogenic differentiation of MSCs (5, 11, 39-44). Recently in the field of tissue engineering, three-dimensional printing (3DP) has emerged as an attractive technique for the development of biphasic, triphasic, and even multiphasic constructs that better mimic the complexities of tissues and interfaces (45-48). The improved understanding of the effects of architectural and compositional aspects of graded constructs on osteogenic differentiation of MSCs will further guide construct design and fabrication for interfacial tissue engineering.

Downloaded by Ucsf Library University of California San Francisco from www.liebertpub.com at 11/08/19. For personal use only.

Tissue Engineering
Multi-Material Dual Gradient 3D Printing for Osteogenic Differentiation and Spatial Segregation (DOI: 10.1089/ten.TEA.2019.0204)
This paper has been peer-reviewed and accepted for publication, but has yet to undergo copyediting and proof correction. The final published version may differ from this proof.

In the present work, 3D printed porous composite PCL-based constructs with vertical gradients in porosity and pore size, as well as ceramic content of β-TCP were fabricated and seeded with MSCs to direct spatially-dependent osteogenic differentiation. The constructs were then evaluated using a variety of biochemical assays to elucidate the individual and combined effects of compositional and architectural gradients on the osteogenic differentiation and mineralized matrix development of MSCs in a 3D culture environment. Specifically, this study focused on the effects of 1) a vertical porosity gradient; 2) a vertical ceramic gradient; and 3) a combined dual vertical porosity/ceramic gradient on the spatiotemporal osteogenic differentiation of cultured MSCs and mineralized matrix deposition.

2. Materials and Methods

2.1. Experimental design

In order to evaluate the specific objectives of the study as outlined above, seven different experimental groups (Table 1) were examined for directing the spatiotemporal osteogenic differentiation of MSCs. As presented in Figure 1, groups either contained uniform architecture and composition, a vertical architectural gradient, a vertical compositional gradient, or a combined vertical architectural/compositional (dual) gradient. The bulk material used for control scaffolds $Pore_U$ and $Pore_G$ was 10 wt% HA in PCL. To observe baseline effects of uniformly increased ceramic content, the bulk material for control scaffolds $TCP10Pore_U$ and $TCP10Pore_G$ was 10 wt% HA and 10 wt% β-TCP in PCL. To elucidate the individual effects of a ceramic gradient, the TCP_GPore_U and TCP_GPore_G groups were composed of three different bulk materials: 0 wt% β-TCP/10 wt% HA in the top section, 10 wt% β-TCP/10 wt% HA in the middle section, and 20 wt% β-TCP/10 wt% HA in the bottom section. The TCP_GPore_U and TCP_GPore_G groups were then compared to the $Pore_U$/$TCP10Pore_U$ and $Pore_G$/$TCP10Pore_G$ groups, respectively. To elucidate the individual effects of a porosity gradient, groups $Pore_U$, $TCP10Pore_U$, and TCP_GPore_U were compared with groups $Pore_G$, $TCP10Pore_G$, and TCP_GPore_G respectively. Finally, the combined effects of a dual porosity/ceramic gradient were evaluated by comparing the first experimental group, TCP_GPore_G, with the uniform porosity and ceramic negative controls, $Pore_U$ and $TCP10Pore_U$. The second experimental group, TCP_GPore_{GI}, was included to additionally observe the effect of an inverted pore gradient relative to the TCP_GPore_G group.

Downloaded by Ucsf Library University of California San Francisco from www.liebertpub.com at 11/08/19. For personal use only.

Tissue Engineering
Multi-Material Dual Gradient 3D Printing for Osteogenic Differentiation and Spatial Segregation (DOI: 10.1089/ten.TEA.2019.0204)

This paper has been peer-reviewed and accepted for publication, but has yet to undergo copyediting and proof correction. The final published version may differ from this proof.

2.2. Fabrication of the 3D Printed β-TCP/HA/PCL Composite Constructs

The 3D printed composite scaffolds were fabricated by adapting previously established protocols in our laboratory (49, 50). Briefly, HA (average particle size 208 nm, Sigma-Aldrich, St. Louis, MO), PCL (nominal molecular weight 50,000 Da, Mn = 41,000 ± 900 Da, Mw = 56,000 ± 1,200 Da, Polysciences, Warrington, PA), and β-TCP (average particle size 237 nm, Sigma-Aldrich, St. Louis, MO) were homogeneously mixed in a mortar and pestle at varying weight percentages, as outlined in Table 1. The molecular weight of PCL was determined using an ACQUITY Advanced Polymer Chromatography as previously described (49). Square models (8 mm x 8 mm x 4.32 mm) were designed in SketchUp (Trimble, Sunnyvale, CA, USA) and sliced at a layer thickness of 0.36 mm in BioplotterRP Software for 3D printing (EnvisionTEC, Gladbeck, Germany). Throughout the document, the word "fiber" is used to describe filaments printed to form each scaffold. Three distinct fiber spacing patterns – 0.2 mm (small, S), 0.6 mm (medium, M), and 1.0 mm (large, L) – were created by altering the spacing between adjacent fibers. β-TCP/HA/PCL mixtures were printed using a 3D Bioplotter (EnvisionTEC) extrusion printer. Printing conditions (pressure, speed, pre- and post-flow, wait time) were set for each composition to maintain a fiber diameter of 400 ± 60 µm (15% quality control window) and are shown in Table 2. To manufacture constructs with porosity gradients, three separate square models corresponding to the selected fiber spacings were stacked within the Bioplotter RP Software and sliced with the same layer thickness as stated above (0.36 mm). Finally, scaffolds that had a compositional gradient were printed in a similar manner, but three separate high temperature cartridges were employed.

2.3. Structural Architecture of 3D Printed Composites

Constructs were analyzed by microcomputed tomography (µCT**)** in order to quantify the fiber diameters and porosity gradient (49, 51). Briefly, 3D printed constructs (n=3) were scanned using a Skyscan 1272 (Ver 1.1.11, Bruker, Kontich, Belgium) at an x-ray voltage and current of 40 kV and 250 µA, respectively. Scans were performed with a rotation step size of 0.6º, 16.0 µm/pixel, frame averaging of 4, and a random movement of 10. Raw images were reconstructed using NReconn (Ver 1.7.1.0, Bruker). In order to determine the fiber size and porosity present in each section of the constructs, a 7.5 mm x 7.5 mm x 1.2 mm region of interest was used in each subsection of the construct and

analyzed in CTan (Ver 1.17.7.2+, Bruker). To determine the fiber diameter in each section, 10 longitudinal slices were randomly selected, and an average fiber diameter for one scaffold section was obtained using n=10 fibers/slice. Group average fiber diameters were obtained using n= 3 sections/group.

2.4. Rabbit Bone Marrow Mesenchymal Stem Cell Harvest

All experimental and surgical protocols were reviewed and approved by the Rice University Institutional Animal Care and Use Committee and were conducted following the animal care and use guidelines set forth by the National Institutes of Health. MSCs were isolated from the bone marrow of 6 month old New Zealand male white rabbits as previously described (52). After induction of anesthesia, bone marrow was aspirated into 10 mL syringes that contained 1000 U of heparin. The bone marrow aspirate was cultured in 225-cm^2 tissue culture flasks for 3 weeks in an incubator at 37 ºC and 5% CO_2, with medium changes every 3 days, in general medium (GM) containing low-glucose Dulbecco's modified Eagle's medium (DMEM-LG), 10% v/v fetal bovine serum (FBS), 1% v/v GlutaMAX, and 1% v/v penicillin/streptomycin/fungizone (PSF). After which, the adherent fraction of cells from the 6 rabbits was pooled in order to minimize inter-animal variability and designated as "MSCs" given the established osteogenic potential of these cells (1, 53). MSCs were expanded in GM and seeded on the constructs at passage four.

2.5. Seeding of 3D Printed Scaffolds

After fabrication, 3D printed constructs were sterilized in a 12 h ethylene oxide cycle (Anprolene AN74i , Anderson Sterilizers, Haw River, NC) and allowed to vent for 24 h prior to cell seeding. Constructs were immersed in a sterile gradient of ethanol and phosphate buffered saline (PBS, Gibco, Waltham, MA) (100, 75, 50, 25 and 0%), washed 3 times with PBS and incubated in 2 mL of complete medium overnight on a shaker table. On the following day, four constructs were placed into a 10 mL syringe with 3 mL of complete medium and a concentration of 5.0 x 10^5 cells/mL measured by a hemocytometer. Syringe plungers were compressed to remove any air and capped with a sterile syringe filter. After which, syringes with the constructs were placed on a rotating wheel (5 RPM) in an incubator for 14 hrs to facilitate cell adhesion. Individual constructs were transferred to 24-well plates (ultralow attachment plates) with 1 mL of complete osteogenic medium (DMEM-LG, 10% v/v FBS, 10 mM β-glycerol-2-phosphate, 10 nM dexamethasone, 50

Downloaded by Ucsf Library University of California San Francisco from www.liebertpub.com at 11/08/19. For personal use only.

Tissue Engineering
Multi-Material Dual Gradient 3D Printing for Osteogenic Differentiation and Spatial Segregation (DOI: 10.1089/ten.TEA.2019.0204)
This paper has been peer-reviewed and accepted for publication, but has yet to undergo copyediting and proof correction. The final published version may differ from this proof.

mg/mL ascorbic acid, 1% v/v GlutaMAX, and 1% v/v PSF) per well, which was exchanged every two days. Seeded constructs were cultured for 3, 14, or 28 days. To evaluate cell proliferation between days 1 and 3 of culture, gradient ceramic constructs (TCP_GPore_U, TCP_GPore_G, and TCP_GPore_{GI} were separately seeded and cultured for 1 or 3 days following the same methods described above.

2.6. Biochemical Assays

After the respective culture periods, constructs were rinsed twice in PBS, cut in half longitudinally, delaminated, and placed into 400 µL of sterile-filtered Millipore water and frozen at -20 ºC for further analysis. Each construct underwent three freeze thaw cycles followed by ultrasonication to lyse the cells in order to assay the delaminated constructs for cellularity and alkaline phosphatase (ALP) activity. The amount of DNA was quantified using a Quant-iT PicoGreen dsDNA Assay Kit (Molecular Probes, Eugene, OR) according to the manufacturer's instructions. Briefly, cell lysate, assay buffer, and dye solution were placed into the well of a black 96-well plate and incubated for 10 min at room temperature. Fluorescence was measured with an excitation wavelength of 490 nm and emission wavelength of 520 nm (BioTek FLX800, Winooski, VT). Following previous established protocols, the amount of DNA present in the cell population used to seed the scaffolds was determined to be 4.4 ± 0.2 pg/cell, using n=3 samples of 100,000 MSCs. Results are expressed as cells per section by normalizing the measured DNA content from experimental samples to this value (54). ALP enzymatic activity was determined according to an established colorimetric assay that relies on the conversion of *para*-nitrophenylphosphate to *para*-nitrophenol (Abcam, Cambridge, MA) (55). In order to measure the calcium content, acetic acid was added to the samples (n=4) with a final concentration of 0.5 M and incubated on a shaker table at room temperature overnight. Calcium arenazo III (Sigma-Aldrich) reagent was then added and the absorbance at 650 nm was measured with a (BioTek Powerwave x340) plate reader. Values were normalized to cell number for each respective delaminated section. Unseeded constructs were incubated under identical conditions as the cultured constructs for 3, 14, and 28 days, at which point the calcium was measured (Figure S1) in order to correct for calcium

Downloaded by Ucsf Library University of California San Francisco from www.liebertpub.com at 11/08/19. For personal use only.

Tissue Engineering
Multi-Material Dual Gradient 3D Printing for Osteogenic Differentiation and Spatial Segregation (DOI: 10.1089/ten.TEA.2019.0204)
This paper has been peer-reviewed and accepted for publication, but has yet to undergo copyediting and proof correction. The final published version may differ from this proof.

deposited from the medium or present within the constructs to ensure that the calcium measured accurately reflected active mineralization by the cultured cells.

2.7. Real-time Reverse Transcription Polymerase Chain Reaction

To evaluate the change of osteogenic genes, constructs were rinsed twice in PBS, delaminated, and cut into small pieces. In order to reproducibly delaminate the constructs, cutting guides were designed using CAD software (Autodesk Inventor, San Rafael, CA) and 3D printed such that a low-profile, 0.26mm thick microtome blade (AccuEdge® 4689) could be used to cut the constructs at the architectural or compositional transition points. The guide referenced the surface of the construct that was adjacent to the printer bed during fabrication in order to ensure sections were flat and parallel to the horizontal faces. Sections of compositions from similar constructs were combined in order to ensure the collection of a sufficient amount of RNA, as has been described previously, placed in an Eppendorf tube with 1 mL of TRIzol (Invitrogen, Carlsbad, CA), and stored at -80 ºC (24). RNA was isolated with a TRIzol Plus RNA Purification Kit (Invitrogen) following the manufacturer's instructions for isolation of RNA from animal cells. The concentration and the purity of RNA were evaluated with a Nanodrop 2000 (Thermo Fisher, Waltham, MA). Reverse transcription was performed using One-Step SYBR™ GreenER™ Kit, with premixed ROX (Invitrogen) and the primers listed in Table 3 (55-57). PCR was performed on the CFX96Touch (Bio-Rad Laboratories, Hercules, CA) under the recommended conditions: cDNA was synthesized at 60 ºC for 10 min, denatured at 95 ºC for 2 min, followed by 40 cycles of 95 ºC for 15 s and 65 ºC for 60 s. The expression of target genes was normalized to the expression of the housekeeping gene glyceraldehyde-3-phosphate dehydrogenase (GAPDH) in the samples (ΔC_t) (n=1). Results are expressed as fold induction in mRNA expression normalized to the gene expression of the MSC cell stock used to seed the scaffolds.

2.8. Histological Processing

Constructs were longitudinally sectioned in half and sent to the MD Anderson Cancer Center Research Histology Core Laboratory (Houston, TX, USA) for embedding and cryosectioning. Sections (5 µm) were taken from the center of the constructs and staining

Downloaded by Ucsf Library University of California San Francisco from www.liebertpub.com at 11/08/19. For personal use only.

Tissue Engineering
Multi-Material Dual Gradient 3D Printing for Osteogenic Differentiation and Spatial Segregation (DOI: 10.1089/ten.TEA.2019.0204)
This paper has been peer-reviewed and accepted for publication, but has yet to undergo copyediting and proof correction. The final published version may differ from this proof.

was performed with von Kossa using a 2% silver nitrate solution incubated under UV for 30 min.

2.9. Confocal Microscopy

After 1 and 3 days in culture, transverse sections (1 mm thick) of constructs were rinsed twice in PBS, fixed in Richard-Allan Scientific Neutral Buffered Formalin (10%) (Thermo Fisher) for 30 min, and permeabilized with CytoVista permeabilization buffer (Invitrogen) for 30 min at room temperature. Samples were then washed three times in CytoVista wash buffer (Invitrogen) for 5 min at room temperature and submerged in Image-IT FX Signal Enhancer (Invitrogen). Samples were then stained for actin with Alexa Fluor 488 Phalloidin (Invitrogen) at a concentration of 6 µL/mL and the nuclei were stained with 4,6-diamidino-2-phenylindole (DAPI; Abcam, Boston, MA) staining solution (2.5 µM in PBS) and washed three times in PBS. Samples were then visualized with a Nikon A1 confocal microscope (Minato, Tokyo, Japan).

2.10. Fluorescence Microscopy

After 1 and 3 days the TCP_GPore_U group was assessed for cell aggregations within the pores by using fluorescence microscopy following previous protocols (58). Briefly, constructs were rinsed twice in PBS, fixed in 4% paraformaldehyde for 30 min, and permeabilized with CytoVista permeabilization buffer (Invitrogen) for 30 min at room temperature. Constructs were stained with Alexa Fluor 488 Phalloidin (Invitrogen) at a concentration of 6 µL/mL and three different sections (top, middle, and bottom) were visualized with a Nikon Ti2-U with a DS-FI3 microscope camera.

2.11. Statistical Analysis

JMP Pro 14 (SAS, Cary, NC) was used to evaluate the data set using a one-way analysis of variance (ANOVA) test with *post hoc* analysis by Tukey's honestly significant difference (HSD). Results were considered significant at $p < 0.05$. Results are presented as means ± standard deviations.

Downloaded by Ucsf Library University of California San Francisco from www.liebertpub.com at 11/08/19. For personal use only.

Tissue Engineering
Multi-Material Dual Gradient 3D Printing for Osteogenic Differentiation and Spatial Segregation (DOI: 10.1089/ten.TEA.2019.0204)
This paper has been peer-reviewed and accepted for publication, but has yet to undergo copyediting and proof correction. The final published version may differ from this proof.

Downloaded by Ucsf Library University of California San Francisco from www.liebertpub.com at 11/08/19. For personal use only.

Tissue Engineering
Multi-Material Dual Gradient 3D Printing for Osteogenic Differentiation and Spatial Segregation (DOI: 10.1089/ten.TEA.2019.0204)
This paper has been peer-reviewed and accepted for publication, but has yet to undergo copyediting and proof correction. The final published version may differ from this proof.

3. Results

3.1. Scaffold Architecture

The average fiber diameters measured for each scaffold section and group are presented in Figure 2. A ±15% quality control window on the desired nominal fiber diameter of 400 µm was applied to all scaffolds. Scaffolds with average fiber diameters outside of this criterion were not included in the study, and replacement scaffolds were printed with the same conditions. As seen in Figure 3, for gradient scaffolds, sections of significantly different ($p < 0.05$) porosities were incorporated by varying the lateral fiber spacing between sections. Specifically, the porosities (Figure 3) of individual zones were 33 ± 4 %, 50 ± 4 %, and 65 ± 3 %for the small (0.2 mm), medium (0.6 mm), and large (1.0 mm) fiber spacings, respectively. Furthermore, among uniform and gradient scaffolds, the porosity of the uniform scaffolds (0.6 mm fiber spacing) was similar ($p > 0.05$) to the porosity of the 0.6 mm zone of gradient scaffolds.

3.2. Cellularity

The cellularity of the constructs was analyzed at days 3, 14, and 28 (Figure 4). At day 3, there was no discernible difference in the cellularity between the individual sections of the constructs ($p > 0.05$). After 14 days, significant differences between sections could be observed. Specifically, sections that contained 20 wt% β-TCP (bottom section of TCP_GPore_U, TCP_GPore_G, and TCP_GPore_{GI}) had lower cell content compared to sections containing 0 wt% β-TCP within the same construct (top section of TCP_GPore_U, TCP_GPore_G, and TCP_GPore_{GI}, $p < 0.05$). In addition, equivalent cellularity was observed between sections of groups that contained a uniform ceramic concentration independent of the pore gradient ($Pore_U$ and $Pore_G$, $TCP10Pore_U$ and $TCP10Pore_G$, $p > 0.05$). At day 28, the majority of sections had similar cellularity ($p > 0.05$). The only noticeable difference was between the top and bottom section of $TCP10Pore_G$ ($p < 0.05$). Finally, the cell distribution is presented in Figure S2, and it was observed that dynamic seeding resulted in a homogenous attachment of cells.

The cellularity of gradient ceramic constructs (TCP_GPore_U, TCP_GPore_G, and TCP_GPore_{GI}) was separately analyzed at days 1 and 3 (Figure S3). At both day 1 and day 3, there were no discernable differences in the cellularity between individual construct sections containing either the same ceramic composition or the same pore architecture ($p > 0.05$).

Downloaded by Ucsf Library University of California San Francisco from www.liebertpub.com at 11/08/19. For personal use only.

Tissue Engineering
Multi-Material Dual Gradient 3D Printing for Osteogenic Differentiation and Spatial Segregation (DOI: 10.1089/ten.TEA.2019.0204)

This paper has been peer-reviewed and accepted for publication, but has yet to undergo copyediting and proof correction. The final published version may differ from this proof.

At day 3, the cellularity of all construct sections trended higher compared to day 1, with statistically significant increases observed in all construct sections containing 20 wt% β-TCP (bottom sections of TCP_GPore_U, TCP_GPore_G, and TCP_GPore_{GI}, $p < 0.05$) as well as the middle section of the TCP_GPore_G group and the top and middle sections of the TCP_GPore_{GI} group ($p < 0.05$). Confocal microscopy of gradient ceramic constructs (TCP_GPore_U, TCP_GPore_G, and TCP_GPore_{GI}, Figure 5) demonstrated uniform spreading of seeded cells across the constructs at day 1. Additionally, fluorescence microscopy of the TCP_GPore_U formulation (Figure S4) demonstrated the formation cell aggregates on top of construct fibers. Additionally, in both Figure 5 and Figure S4, cellular material can be observed extending into the construct pores.

3.3. ALP Activity

To evaluate the early commitment to osteogenic differentiation, ALP activity was measured at days 3, 14, and 28 (Figure 6). At day 14, equivalent ALP activity was observed between sections of scaffolds that contained 0 wt% β-TCP ($Pore_U$ vs. $Pore_G$, $p > 0.05$) and 10 wt% β-TCP ($TCP10Pore_U$ vs. $TCP10Pore_G$, $p > 0.05$), while a significantly higher ALP activity was observed in the sections containing 20 wt% β-TCP when compared to the 0 wt% β-TCP sections within the same construct for groups with a β-TCP gradient (TCP_GPore_G, and TCP_GPore_{GI}, $p < 0.05$). A temporal increase in ALP activity was observed at day 14 in groups that contained a ceramic gradient independent of the presence of a porosity gradient compared to the same sections at 3 days (TCP_GPore_U, TCP_GPore_G, and TCP_GPore_{GI}, $p < 0.05$). Finally, peak ALP activity was observed at day 14 in groups that contained a ceramic gradient (TCP_GPore_U, TCP_GPore_G, and TCP_GPore_{GI}, $p < 0.05$) followed by a decrease in ALP activity at day 28.

3.4. Osteogenic Differentiation

To understand the effects of physical and biochemical gradients on early and late osteogenic differentiation, quantitative RT-PCR for specific osteogenic markers was performed (Figures 7, 8, 9). Maximum *Runx2* expression (Figure 7) was observed in all groups at day 3 followed by a decline for the remainder of the study. The concentration of β-TCP appeared to affect the up-regulation of *Runx2* at day 3. Specifically, the expression level of *Runx2* trended higher in sections that contained 20 wt% β-TCP compared to sections that contained 0 wt% β-TCP within the same construct (TCP_GPore_U, TCP_GPore_G,

Downloaded by Ucsf Library University of California San Francisco from www.liebertpub.com at 11/08/19. For personal use only.

Tissue Engineering
Multi-Material Dual Gradient 3D Printing for Osteogenic Differentiation and Spatial Segregation (DOI: 10.1089/ten.TEA.2019.0204)
This paper has been peer-reviewed and accepted for publication, but has yet to undergo copyediting and proof correction. The final published version may differ from this proof.

and TCP_GPore_{GI}). Within the $TCP10Pore_G$ group at day 3, the highest porosity section appeared to demonstrate an up-regulation of *Runx2* compared to the lowest porosity section, although the effect of porosity on *Runx2* expression was not observed for the $Pore_G$ group. At day 3 the expressions of late osteogenic differentiation (osteopontin (*Opn*, Figure 8) and osteocalcin (*Ocn*, Figure 9)) was similar. However, at day 14, scaffold sections containing 20 wt% β-TCP and the highest porosity (bottom section of TCP_GPore_G) tended to have higher expression of *Opn*. While the apparent upregulation of *Opn* due to β-TCP concentration was observed after 14 days, the impact of porosity on trends in *Opn* expression was not observed until day 28. Specifically, at 28 days in both the $Pore_G$ and $TCP10Pore_G$ groups, sections of higher porosity tended to have up-regulated *Opn* levels compared to sections of lower porosity. Finally, a temporal increase in *Opn* expression was observed for sections that had at least 10 wt% β-TCP present. Regarding *Ocn* expression (Figure 9), up-regulation was observed in all groups after 14 days with maximum expression detected at day 28. Also, increasing concentration of β-TCP from 0 to 20 wt% resulted in an upward trend in *Ocn* expression after day 14.

3.5. Mineralized Matrix

A calcium deposition assay (Figure 10 and Figure 11) was used in order to assess the amount of mineralized matrix, which is considered to be evidence of full osteogenic maturation (59). At all timepoints, no spatial differences in mineralization were observed between sections of groups with uniform porosity and composition ($Pore_U$ and $TCP10Pore_U$, $p > 0.05$) (Figure 10). At 14 days, MSCs that were seeded in sections that contained higher concentrations of β-TCP demonstrated higher levels of mineralization per cell. Specifically, layers that contained 20 wt% β-TCP had significantly higher mineralization when compared to layers that contained 0 wt% or 10 wt% β-TCP (TCP_GPore_U and TCP_GPore_{GI}, $p < 0.05$). In fact, a 2-fold increase of total ceramic content after the addition of β-TCP resulted in over a 10-fold increase in mineralization after 14 days ($Pore_U$ vs. $TCP10Pore_U$). Interestingly, at 14 days there were no observable differences in mineralization between groups that only had a pore gradient compared to their respective uniform pore controls ($Pore_U$ and $Pore_G$, $TCP10Pore_U$ and $TCP10Pore_G$, $p > 0.05$). After 28 days, the section that contained 20 wt% β-TCP and the highest porosity (bottom section of TCP_GPore_G) had a higher level of mineralization (on a per cell basis) than any other section

($p < 0.05$) (Figure 11). Finally, differences in mineralization were detected after 28 days between sections that contained the highest and lowest porosity in uniform ceramic, gradient porosity constructs ($Pore_G$ and $TCP10Pore_G$, $p < 0.05$). Representative histological sections at 28 days are presented in Figure S5 in order to visualize the amount of mineralization. It was observed that increasing concentrations of β-TCP resulted in enhanced mineralization, as noted by the enhanced black staining around the perimeter of the pores.

4. Discussion

In the present study, porous 3D printed composite PCL-based constructs with vertical gradients in porosity and β-TCP concentration were fabricated, in order to create osteoblastic phenotypic gradients of MSCs for the generation of complex heterogenous constructs. Specifically, the study focused on the effects of 1) a vertical porosity gradient; 2) a vertical ceramic gradient of β-TCP; and 3) a combined dual porosity/ceramic gradient on the generation of phenotypic gradients of seeded MSCs by individually evaluating separate construct sections. To this end, three different concentrations of β-TCP (0, 10, and 20 wt%) and three different porosities (33 ± 4 %, 50 ± 4 %, and 65 ± 3 %) were investigated. The results of this study demonstrated distinct differences in the osteogenic differentiation of MSCs depending on their spatial location within graded constructs. In particular, regions with the highest concentrations of β-TCP (20 wt%) stimulated mineralization in comparison to sections with the lowest concentration of β-TCP (0 wt%) at days 14 and 28, independent of pore size. However, differences in mineralization were not observed until day 28 for regions that had differing porosities but uniform β-TCP concentrations.

Early and late markers of osteogenic differentiation were assayed to understand the effects of β-TCP concentration and construct porosity on the osteogenic differentiation of MSCs. Specifically, ALP and *Runx2* are early transient markers of osteogenic differentiation, while mineralization, *Opn*, and *Ocn* are indicative of late-stage osteogenic differentiation (60, 61). The paradigmatic increase and subsequent decrease of ALP activity was observed in all groups with peak ALP activity observed at day 14. ALP activity between different construct sections was found to be directly related to the amount of β-TCP present within

Downloaded by Ucsf Library University of California San Francisco from www.liebertpub.com at 11/08/19. For personal use only.

Tissue Engineering
Multi-Material Dual Gradient 3D Printing for Osteogenic Differentiation and Spatial Segregation (DOI: 10.1089/ten.TEA.2019.0204)
This paper has been peer-reviewed and accepted for publication, but has yet to undergo copyediting and proof correction. The final published version may differ from this proof.

Downloaded by Ucsf Library University of California San Francisco from www.liebertpub.com at 11/08/19. For personal use only.

Tissue Engineering
Multi-Material Dual Gradient 3D Printing for Osteogenic Differentiation and Spatial Segregation (DOI: 10.1089/ten.TEA.2019.0204)
This paper has been peer-reviewed and accepted for publication, but has yet to undergo copyediting and proof correction. The final published version may differ from this proof.

those sections but independent of the porosity. This observation indicates that, during early osteogenic lineage development, β-TCP concentration more strongly influences MSC differentiation towards an osteoblastic phenotype compared to porosity.

In a previous study, Takahashi *et al.* demonstrated that β-TCP had a positive, dose-dependent effect on the osteogenic differentiation of MSCs that were cultured within gelatin sponges (62). Similarly, a recent study by Diaz-Gomez *et al.* demonstrated a dose-dependent effect of HA composition on calcium deposition when radially gradient PCL-based scaffolds were incubated in simulated body fluid. Specifically, outermost sections of 30 wt% HA/PCL demonstrated increased calcium deposition compared to middle sections of 15 wt% HA/PCL and inner sections of pure PCL (63). In the present study, a dose-dependent effect of β-TCP on mineralization and ALP activity was shown. Furthermore, several studies have observed that β-TCP initiates osteogenic differentiation within 3 days (64-66). These observations corroborate with the results of the present study, as significant dose-dependent upregulation of the osteogenic marker ALP was observed as early as 3 days. Also, the further increase in osteogenic differentiation seen in sections with a higher concentration of β-TCP may be explained by the dissolution of calcium ions, which have been shown to play a critical role on the osteogenic differentiation of MSCs. Specifically, extracellular calcium activates Class C G protein-coupled calcium-sensing receptors, increasing the expression of type L voltage-gated calcium channels (67, 68). This channel activation triggers a signaling cascade that leads to the upregulation of bone morphogenetic protein-2 (BMP-2) and thus enhanced osteogenic differentiation (69-71).

No differences in ALP activity expression were observed between sections of uniform material, gradient porosity constructs ($Pore_G$ and $TCP10Pore_G$). However, within the uniform material, gradient porosity constructs, sections with higher porosity displayed enhanced markers of late osteogenic differentiation compared to sections with lower porosity. These observations imply that porosity predominately influences late-stage osteogenic differentiation, which is characterized by the degree of mineralization, rather than early-stage osteogenic differentiation.

The mineralization of all groups monotonically increased over the course of the study. On a per-section basis, the sections with 20 wt% β-TCP (TCP_GPore_U, TCP_GPore_G, and TCP_GPore_{GI}) resulted in the highest amounts of mineralized matrix again corroborating the

Downloaded by Ucsf Library University of California San Francisco from www.liebertpub.com at 11/08/19. For personal use only.

Tissue Engineering
Multi-Material Dual Gradient 3D Printing for Osteogenic Differentiation and Spatial Segregation (DOI: 10.1089/ten.TEA.2019.0204)
This paper has been peer-reviewed and accepted for publication, but has yet to undergo copyediting and proof correction. The final published version may differ from this proof.

influence of β-TCP on the osteogenic differentiation. However, normalizing to the cell number present in each section, one can see that the combination of 20 wt% β-TCP and the highest porosity (TCP_GPore_G) resulted in the greatest amount of mineralized matrix per cell. This specific observation again demonstrates the influence of porosity on late-stage osteogenic differentiation. The mineralization observed in the present study is similar to that of previous *in vitro* studies that investigated PCL-based constructs for bone tissue engineering (72-75). After 28 days in the present study, regions with higher porosity within uniform composition constructs demonstrated enhanced osteogenic differentiation and mineralization, further supporting the hypothesis that porosity affects osteogenesis at later stages as has been shown previously (76-79). It has been hypothesized that the presence of larger pores facilitates the migration of cells and diffusion of bioactive molecules leading to a more mature osteogenic phenotype (80). Matsko *et al.* postulated that cell morphology can also drive the differences seen in the cellular response due to scaffold porosity since the process of differentiation is known to be dependent upon cell morphology (81, 82). Another plausible explanation for the differences in the osteoblastic phenotype between sections with smaller and larger pores could be due to diffusion limitations within the smaller pores as a result of the cell aggregates present at day 1 and 3. It has been postulated that cells are more likely to remain in a pluripotent state when nutrients are limited due to diffusion (83).

In gradient composition constructs (TCP_GPore_U, TCP_GPore_G, and TCP_GPore_{GI}), porosity had a comparatively lower effect on markers of late-stage osteogenic differentiation than uniform composition constructs ($Pore_G$ and $TCP10Pore_G$). This observation suggests that β-TCP concentration was the dominant factor in influencing the osteogenic differentiation of MSCs under the conditions in the preset study. One plausible explanation for a phenotypic gradient driven by a gradient in ceramic content as observed in this study is the selective adsorption of proteins and other soluble factors, whether added to the media or secreted by seeded cells, to scaffold sections of higher ceramic concentration. It has been widely demonstrated that protein adsorption to a scaffold surface is highly dependent on the physicochemical makeup of that surface (84). As applied to bone tissue formation and mineralization, proteins often demonstrate a selective affinity to surfaces with calcium phosphate moieties (85). A similar ceramic dose-dependent phenomenon was observed in

Downloaded by Ucsf Library University of California San Francisco from www.liebertpub.com at 11/08/19. For personal use only.

Tissue Engineering
Multi-Material Dual Gradient 3D Printing for Osteogenic Differentiation and Spatial Segregation (DOI: 10.1089/ten.TEA.2019.0204)
This paper has been peer-reviewed and accepted for publication, but has yet to undergo copyediting and proof correction. The final published version may differ from this proof.

the radial gradient study by Diaz-Gomez *et al.*, where regions of higher HA composition led to increased calcium deposition despite significantly lower porosity in the outer regions containing a high HA composition compared to inner regions with lower or no HA content (63).

We have previously demonstrated how 3D printing can be leveraged to fabricate a wide range of complex multiphasic constructs (49-51). As such, the most notable result from this study is that by altering the porosity and ceramic composition within a construct, one can direct the osteoblastic phenotype of MSCs within distinct regions of the construct in order to create cell phenotype gradients. Furthermore, it was observed that the spatial orientation of the sections influenced the osteogenic differentiation of adjacent layers. In fact, sections that contained 0 wt% β-TCP within compositional gradient constructs (TCP_GPore_U, TCP_GPore_G, and TCP_GPore_{GI}) had a higher level of mineralization compared to 0 wt% β-TCP sections within uniform composition constructs ($TCP10Pore_U$ and $TCP10Pore_G$).

We acknowledge that the present study had several limitations. While an inverse pore gradient group (TCP_GPore_{GI}) was included in the study, the 20 wt% β-TCP section was always located on the bottom of the construct. As a result, it is difficult to determine if the enhanced osteogenic differentiation observed in the 20 wt% β-TCP sections was due to the ceramic concentration independent of orientation. As such, it would be interesting to investigate the effects of an inverse compositional gradient in order to further understand this observation. We also acknowledge that the literature surrounding bone infill in tissue engineering has identified pore sizes >300μm to be optimal for bone tissue engineering scaffolds (86). However, the scope of this study was to investigate topological changes observed during osteogenic differentiation caused by gradients in pore size and ceramic content. The results from the study demonstrate the physicochemical properties of each parameter and significant differences between different scaffold sections, highlighting the importance of gradients in tissue engineered scaffolds.

Additionally, the timepoints selected for the present study were ideal for measuring end-stage mineralization, as previously outlined in the objectives. Therefore, since ALP and *Runx2* are transient markers of osteogenic differentiation it is possible that the time points selected did not capture global peak expression during the culture period, but rather a local maximum. However, in the present study the cellularity of the constructs was not

Downloaded by Ucsf Library University of California San Francisco from www.liebertpub.com at 11/08/19. For personal use only.

Tissue Engineering
Multi-Material Dual Gradient 3D Printing for Osteogenic Differentiation and Spatial Segregation (DOI: 10.1089/ten.TEA.2019.0204)
This paper has been peer-reviewed and accepted for publication, but has yet to undergo copyediting and proof correction. The final published version may differ from this proof.

dependent on the surface area of an individual section. This is likely due to the cell aggregates that formed within the pore spaces during the seeding of the scaffolds. While the constructs had exhibited a high rate of proliferation between days 1 and 3, after day 3 the cellularity did not change for the remainder of the study. It is well established that cell proliferation and differentiation are inversely related processes (87). As an immature cell begins to differentiate into more a mature phenotype, especially in the presence of osteogenic cell culture supplements, there is a restriction in the cellular proliferative capacity. Ultimately the tissue architecture and function are dependent upon the maintenance of cell-cycle arrest in a terminally differentiated cell (88). Therefore, one plausible explanation for the observed plateau in cell proliferation, after 3 days, is that the cells began differentiating down an osteogenic lineage by day 3, which is supported by the increased expression observed in ALP. Finally, as described in the Materials and Methods section, similar construct sections of the same formulation were combined for biochemical analysis by RT-PCR to ensure a sufficient amount of RNA was collected. As the reported values *Runx2*, *Ocn*, and *Opn* presented here represent the means of replicates, no inferences of statistical significance can be drawn; however, the results align with prior observations in the literature as well as the more definite indications of osteogenic differentiation (ALP activity, and particularly calcium deposition) observed in this study.

The results of this study demonstrated that both β-TCP and porosity can be leveraged to influence the osteogenic differentiation of MSCs that are seeded in a 3D system, leading to the development of heterogenous graded tissue with phenotypic gradients. Furthermore, this study underscores the importance additive manufacturing plays in further controlling and harnessing the interactions between cells and biomaterials for the generation of complex heterogenous tissues and interfaces.

Conclusion

The present study demonstrates that the osteogenic differentiation of MSCs seeded on porous 3D polymeric constructs can be precisely controlled by modulating the local concentration of β-TCP and the construct porosity. Expression of osteogenic markers was stimulated by an increased concentration of β-TCP and a higher porosity for early and late stage osteogenesis, respectively. In particular, significantly higher ALP activity was

observed in 20 wt% β-TCP sections compared to 0 wt% β-TCP sections within ceramic gradient constructs, and these constructs likewise demonstrated a characteristic temporal increase and subsequent decrease in ALP activity. Similarly, at both day 14 and day 28 sections that contained 20 wt% β-TCP had significantly higher mineralization than other sections of the same construct, while in uniform ceramic constructs a 2-fold increase of total ceramic content resulted in over a 10-fold increase in mineralization at day 14. Finally, at day 28 significant differences in mineralization were observed between sections of highest and lowest porosity within pore gradient scaffolds. Also, the spatial arrangement of the layers, which was well-controlled by a 3D printing fabrication strategy, was shown to affect the osteogenic differentiation. The observations from this study suggest that inclusion of β-TCP in HA/PCL constructs enhances markers of both early and late osteogenic differentiation, while construct porosity additionally affects markers of late osteogenic differentiation. Furthermore, differences in construct composition and architecture yielded heterogeneous population of cells within the same construct. These results highlight the potential utility of multiphasic ceramic/polymeric composite constructs for the generation of complex heterogeneous tissues and interfaces.

Downloaded by Ucsf Library University of California San Francisco from www.liebertpub.com at 11/08/19. For personal use only.

Tissue Engineering
Multi-Material Dual Gradient 3D Printing for Osteogenic Differentiation and Spatial Segregation (DOI: 10.1089/ten.TEA.2019.0204)
This paper has been peer-reviewed and accepted for publication, but has yet to undergo copyediting and proof correction. The final published version may differ from this proof.

Acknowledgements

We acknowledge support by the National Institutes of Health (P41 EB023833 and R01 AR068073) and the RegenMed Development Organization (2017-601-002) in the preparation of this work. We also acknowledge the assistance of Gabriel Vazquez Velez for his assistance on RT-PCR. S.M.B. and M.M.S. also acknowledge support from the National Science Foundation Graduate Research Fellowship Program. B.T.S., E.W., and E.R.M. received support from Ruth L. Kirschstein Fellowships from the National Institute of Arthritis and Musculoskeletal and Skin Diseases (F30 AR071258), the National Institute of Dental and Craniofacial Research (F31 DE027586), and the National Cancer Institute (F31 CA213994), respectively. B.T.S., E.W., and E.R.M. acknowledge the Baylor College of Medicine Medical Scientist Training Program. L.D.-G. acknowledges Consellería de Cultura, Educación e Ordenación Universitaria for a Postdoctoral Fellowship (Xunta de Galicia, ED481B 2017/063). Finally, we acknowledge the MD Anderson Cancer Center Research Histology Core Laboratory (NCI CA16672).

Disclosure Statement

No competing financial interests exist.

Downloaded by Ucsf Library University of California San Francisco from www.liebertpub.com at 11/08/19. For personal use only.

Tissue Engineering
Multi-Material Dual Gradient 3D Printing for Osteogenic Differentiation and Spatial Segregation (DOI: 10.1089/ten.TEA.2019.0204)
This paper has been peer-reviewed and accepted for publication, but has yet to undergo copyediting and proof correction. The final published version may differ from this proof.

Downloaded by Ucsf Library University of California San Francisco from www.liebertpub.com at 11/08/19. For personal use only.

Tissue Engineering
Multi-Material Dual Gradient 3D Printing for Osteogenic Differentiation and Spatial Segregation (DOI: 10.1089/ten.TEA.2019.0204)

This paper has been peer-reviewed and accepted for publication, but has yet to undergo copyediting and proof correction. The final published version may differ from this proof.

References

1. Thibault, R.A., Scott Baggett, L., Mikos, A.G., and Kasper, F.K. Osteogenic Differentiation of Mesenchymal Stem Cells on Pregenerated Extracellular Matrix Scaffolds in the Absence of Osteogenic Cell Culture Supplements. Tissue Eng Part A **16**, 431, 2010.

2. Keating, J.F., and McQueen, M.M. Substitutes for Autologous Bone Graft in Orthopaedic Trauma. J Bone Joint Surg Br **83**, 3, 2001.

3. Habibovic, P., and de Groot, K. Osteoinductive Biomaterials--Properties and Relevance in Bone Repair. J Tissue Eng Regen Med **1**, 25, 2007.

4. Lu, H.H., Subramony, S.D., Boushell, M.K., and Zhang, X. Tissue Engineering Strategies for the Regeneration of Orthopedic Interfaces. Ann Biomed Eng **38**, 2142, 2010.

5. Bracaglia, L.G., Smith, B.T., Watson, E., Arumugasaamy, N., Mikos, A.G., and Fisher, J.P. 3d Printing for the Design and Fabrication of Polymer-Based Gradient Scaffolds. Acta Biomater **56**, 3, 2017.

6. Bayraktar, H.H., Morgan, E.F., Niebur, G.L., Morris, G.E., Wong, E.K., and Keaveny, T.M. Comparison of the Elastic and Yield Properties of Human Femoral Trabecular and Cortical Bone Tissue. J Biomech **37**, 27, 2004.

7. Oftadeh, R., Perez-Viloria, M., Villa-Camacho, J.C., Vaziri, A., and Nazarian, A. Biomechanics and Mechanobiology of Trabecular Bone: A Review. J Biomech Eng **137**, 010802, 2015.

8. Gong, J.K., Arnold, J.S., and Cohn, S.H. Composition of Trabecular and Cortical Bone. Anat Rec **149**, 325, 1964.

9. Wegst, U.G., Bai, H., Saiz, E., Tomsia, A.P., and Ritchie, R.O. Bioinspired Structural Materials. Nat Mater **14**, 23, 2015.

10. Sikavitsas, V.I., Temenoff, J.S., and Mikos, A.G. Biomaterials and Bone Mechanotransduction. Biomaterials **22**, 2581, 2001.

11. Bittner, S.M., Guo, J.L., Melchiorri, A., and Mikos, A.G. Three-Dimensional Printing of Multilayered Tissue Engineering Scaffolds. Mater Today **21**, 861, 2018.

12. Yousefi, A.M., Hoque, M.E., Prasad, R.G., and Uth, N. Current Strategies in Multiphasic Scaffold Design for Osteochondral Tissue Engineering: A Review. J Biomed Mater Res A **103**, 2460, 2015.

13. Oh, S.H., Kim, T.H., and Lee, J.H. Creating Growth Factor Gradients in Three Dimensional Porous Matrix by Centrifugation and Surface Immobilization. Biomaterials **32**, 8254, 2011.

14. Bittner, S.M., Guo, J.L., and Mikos, A.G. Spatiotemporal Control of Growth Factors in Three-Dimensional Printed Scaffolds. Bioprinting **12**, e00032, 2018.

15. Ilkhanizadeh, S., Teixeira, A.I., and Hermanson, O. Inkjet Printing of Macromolecules on Hydrogels to Steer Neural Stem Cell Differentiation. Biomaterials **28**, 3936, 2007.

16. Seidi, A., Ramalingam, M., Elloumi-Hannachi, I., Ostrovidov, S., and Khademhosseini, A. Gradient Biomaterials for Soft-to-Hard Interface Tissue Engineering. Acta Biomater **7**, 1441, 2011.

17. Han, F., Zhou, F., Yang, X., Zhao, J., Zhao, Y., and Yuan, X. A Pilot Study of Conically Graded Chitosan-Gelatin Hydrogel/Plga Scaffold with Dual-Delivery of Tgf-Beta1 and Bmp-2 for Regeneration of Cartilage-Bone Interface. J Biomed Mater Res Part B **103**, 1344, 2015.

18. Mikos, A.G., Herring, S.W., Ochareon, P., Elisseeff, J., Lu, H.H., Kandel, R., Schoen, F.J., Toner, M., Mooney, D., Atala, A., Van Dyke, M.E., Kaplan, D., and Vunjak-Novakovic, G. Engineering Complex Tissues. Tissue Eng **12**, 3307, 2006.

19. Lipner, J., Shen, H., Cavinatto, L., Liu, W., Havlioglu, N., Xia, Y., Galatz, L.M., and Thomopoulos, S. In Vivo Evaluation of Adipose-Derived Stromal Cells Delivered with a Nanofiber Scaffold for Tendon-to-Bone Repair. Tissue Eng Part A **21**, 2766, 2015.

Downloaded by Ucsf Library University of California San Francisco from www.liebertpub.com at 11/08/19. For personal use only.

Tissue Engineering
Multi-Material Dual Gradient 3D Printing for Osteogenic Differentiation and Spatial Segregation (DOI: 10.1089/ten.TEA.2019.0204)
This paper has been peer-reviewed and accepted for publication, but has yet to undergo copyediting and proof correction. The final published version may differ from this proof.

20. Kameda, T., Koike, C., Saitoh, K., Kuroiwa, A., and Iba, H. Developmental Patterning in Chondrocytic Cultures by Morphogenic Gradients: Bmp Induces Expression of Indian Hedgehog and Noggin. Genes Cells **4**, 175, 1999.

21. Phillips, J.E., Burns, K.L., Le Doux, J.M., Guldberg, R.E., and Garcia, A.J. Engineering Graded Tissue Interfaces. Proc Natl Acad Sci U S A **105**, 12170, 2008.

22. Roy, T.D., Simon, J.L., Ricci, J.L., Rekow, E.D., Thompson, V.P., and Parsons, J.R. Performance of Degradable Composite Bone Repair Products Made Via Three-Dimensional Fabrication Techniques. J Biomed Mater Res A **66**, 283, 2003.

23. O'Brien, F.J., Harley, B.A., Waller, M.A., Yannas, I.V., Gibson, L.J., and Prendergast, P.J. The Effect of Pore Size on Permeability and Cell Attachment in Collagen Scaffolds for Tissue Engineering. Technol Health Care **15**, 3, 2007.

24. Di Luca, A., Ostrowska, B., Lorenzo-Moldero, I., Lepedda, A., Swieszkowski, W., Van Blitterswijk, C., and Moroni, L. Gradients in Pore Size Enhance the Osteogenic Differentiation of Human Mesenchymal Stromal Cells in Three-Dimensional Scaffolds. Sci Rep **6**, 22898, 2016.

25. Story, B.J., Wagner, W.R., Gaisser, D.M., Cook, S.D., and Rust-Dawicki, A.M. In Vivo Performance of a Modified Csti Dental Implant Coating. Int J Oral Maxillofac Implants **13**, 749, 1998.

26. Kruyt, M.C., de Bruijn, J.D., Wilson, C.E., Oner, F.C., van Blitterswijk, C.A., Verbout, A.J., and Dhert, W.J. Viable Osteogenic Cells Are Obligatory for Tissue-Engineered Ectopic Bone Formation in Goats. Tissue Eng **9**, 327, 2003.

27. Kim, K., Dean, D., Mikos, A.G., and Fisher, J.P. Effect of Initial Cell Seeding Density on Early Osteogenic Signal Expression of Rat Bone Marrow Stromal Cells Cultured on Cross-Linked Poly(Propylene Fumarate) Disks. Biomacromolecules **10**, 1810, 2009.

Downloaded by Ucsf Library University of California San Francisco from www.liebertpub.com at 11/08/19. For personal use only.

Tissue Engineering
Multi-Material Dual Gradient 3D Printing for Osteogenic Differentiation and Spatial Segregation (DOI: 10.1089/ten.TEA.2019.0204)
This paper has been peer-reviewed and accepted for publication, but has yet to undergo copyediting and proof correction. The final published version may differ from this proof.

28. Murphy, C.M., Haugh, M.G., and O'Brien, F.J. The Effect of Mean Pore Size on Cell Attachment, Proliferation and Migration in Collagen-Glycosaminoglycan Scaffolds for Bone Tissue Engineering. Biomaterials **31**, 461, 2010.

29. Kim, S.S., Ahn, K.M., Park, M.S., Lee, J.H., Choi, C.Y., and Kim, B.S. A Poly(Lactide-Co-Glycolide)/Hydroxyapatite Composite Scaffold with Enhanced Osteoconductivity. J Biomed Mater Res A **80**, 206, 2007.

30. Mano, J.F., Sousa, R.A., Boesel, L.F., Neves, N.M., and Reis, R.L. Bioinert, Biodegradable and Injectable Polymeric Matrix Composites for Hard Tissue Replacement: State of the Art and Recent Developments. Compos Sci Technol **64**, 789, 2004.

31. Liao, H.T., Lee, M.Y., Tsai, W.W., Wang, H.C., and Lu, W.C. Osteogenesis of Adipose-Derived Stem Cells on Polycaprolactone-Beta-Tricalcium Phosphate Scaffold Fabricated Via Selective Laser Sintering and Surface Coating with Collagen Type I. J Tissue Eng Regen Med **10**, E337, 2016.

32. Park, C.-H., Kim, E.K., Tijing, L.D., Amarjargal, A., Pant, H.R., Kim, C.S., and Shon, H.K. Preparation and Characterization of La/Pcl Composite Fibers Containing Beta Tricalcium Phosphate (B-Tcp) Particles. Ceram Int **40**, 5049, 2014.

33. Yeo, M., Lee, H., and Kim, G. Three-Dimensional Hierarchical Composite Scaffolds Consisting of Polycaprolactone, Beta-Tricalcium Phosphate, and Collagen Nanofibers: Fabrication, Physical Properties, and in Vitro Cell Activity for Bone Tissue Regeneration. Biomacromolecules **12**, 502, 2011.

34. Lohfeld, S., Cahill, S., Barron, V., McHugh, P., Durselen, L., Kreja, L., Bausewein, C., and Ignatius, A. Fabrication, Mechanical and in Vivo Performance of Polycaprolactone/Tricalcium Phosphate Composite Scaffolds. Acta Biomater **8**, 3446, 2012.

35. Azevedo, M.C., Reis, R.L., Claase, M.B., Grijpma, D.W., and Feijen, J. Development and Properties of Polycaprolactone/Hydroxyapatite Composite Biomaterials. J Mater Sci Mater Med **14**, 103, 2003.

Downloaded by Ucsf Library University of California San Francisco from www.liebertpub.com at 11/08/19. For personal use only.

Tissue Engineering
Multi-Material Dual Gradient 3D Printing for Osteogenic Differentiation and Spatial Segregation (DOI: 10.1089/ten.TEA.2019.0204)
This paper has been peer-reviewed and accepted for publication, but has yet to undergo copyediting and proof correction. The final published version may differ from this proof.

36. Shalumon, K.T., Sowmya, S., Sathish, D., Chennazhi, K.P., Nair, S.V., and Jayakumar, R. Effect of Incorporation of Nanoscale Bioactive Glass and Hydroxyapatite in Pcl/Chitosan Nanofibers for Bone and Periodontal Tissue Engineering. J Biomed Nanotechnol **9**, 430, 2013.

37. Guarino, V., Causa, F., Netti, P.A., Ciapetti, G., Pagani, S., Martini, D., Baldini, N., and Ambrosio, L. The Role of Hydroxyapatite as Solid Signal on Performance of Pcl Porous Scaffolds for Bone Tissue Regeneration. J Biomed Mater Res Part B **86**, 548, 2008.

38. Roohani-Esfahani, S.I., Nouri-Khorasani, S., Lu, Z., Appleyard, R., and Zreiqat, H. The Influence Hydroxyapatite Nanoparticle Shape and Size on the Properties of Biphasic Calcium Phosphate Scaffolds Coated with Hydroxyapatite-Pcl Composites. Biomaterials **31**, 5498, 2010.

39. Ohgushi, H., Okumura, M., Tamai, S., Shors, E.C., and Caplan, A.I. Marrow Cell Induced Osteogenesis in Porous Hydroxyapatite and Tricalcium Phosphate: A Comparative Histomorphometric Study of Ectopic Bone Formation. J Biomed Mater Res **24**, 1563, 1990.

40. Bergmann, C., Lindner, M., Zhang, W., Koczur, K., Kirsten, A., Telle, R., and Fischer, H. 3d Printing of Bone Substitute Implants Using Calcium Phosphate and Bioactive Glasses. J Eur Ceram Soc **30**, 2563, 2010.

41. Bergmann, C.J., Odekerken, J.C., Welting, T.J., Jungwirth, F., Devine, D., Boure, L., Zeiter, S., van Rhijn, L.W., Telle, R., Fischer, H., and Emans, P.J. Calcium Phosphate Based Three-Dimensional Cold Plotted Bone Scaffolds for Critical Size Bone Defects. Biomed Res Int **2014**, 852610, 2014.

42. Inzana, J.A., Olvera, D., Fuller, S.M., Kelly, J.P., Graeve, O.A., Schwarz, E.M., Kates, S.L., and Awad, H.A. 3d Printing of Composite Calcium Phosphate and Collagen Scaffolds for Bone Regeneration. Biomaterials **35**, 4026, 2014.

43. Lin, L., Chow, K.L., and Leng, Y. Study of Hydroxyapatite Osteoinductivity with an Osteogenic Differentiation of Mesenchymal Stem Cells. J Biomed Mater Res A **89**, 326, 2009.

Downloaded by Ucsf Library University of California San Francisco from www.liebertpub.com at 11/08/19. For personal use only.

Tissue Engineering
Multi-Material Dual Gradient 3D Printing for Osteogenic Differentiation and Spatial Segregation (DOI: 10.1089/ten.TEA.2019.0204)
This paper has been peer-reviewed and accepted for publication, but has yet to undergo copyediting and proof correction. The final published version may differ from this proof.

44. Samavedi, S., Whittington, A.R., and Goldstein, A.S. Calcium Phosphate Ceramics in Bone Tissue Engineering: A Review of Properties and Their Influence on Cell Behavior. Acta Biomater **9**, 8037, 2013.

45. Szpalski, C., Wetterau, M., Barr, J., and Warren, S.M. Bone Tissue Engineering: Current Strategies and Techniques--Part I: Scaffolds. Tissue Eng Part B Rev **18**, 246, 2012.

46. Spalazzi, J.P., Dagher, E., Doty, S.B., Guo, X.E., Rodeo, S.A., and Lu, H.H. In Vivo Evaluation of a Multiphased Scaffold Designed for Orthopaedic Interface Tissue Engineering and Soft Tissue-to-Bone Integration. J Biomed Mater Res A **86**, 1, 2008.

47. Dorozhkin, S.V. Biphasic, Triphasic and Multiphasic Calcium Orthophosphates. Acta Biomater **8**, 963, 2012.

48. Catledge, S.A., Clem, W.C., Shrikishen, N., Chowdhury, S., Stanishevsky, A.V., Koopman, M., and Vohra, Y.K. An Electrospun Triphasic Nanofibrous Scaffold for Bone Tissue Engineering. Biomed Mater **2**, 142, 2007.

49. Diaz-Gomez, L., Smith, B.T., Kontoyiannis, P.D., Bittner, S.M., Melchiorri, A.J., and Mikos, A.G. Multimaterial Segmented Fiber Printing for Gradient Tissue Engineering. Tissue Eng Part C Methods **25**, 12, 2019.

50. Bittner, S.M., Smith, B.T., Diaz-Gomez, L., Hudgins, C.D., Melchiorri, A.J., Scott, D.W., Fisher, J.P., and Mikos, A.G. Fabrication and Mechanical Characterization of 3d Printed Vertical Uniform and Gradient Scaffolds for Bone and Osteochondral Tissue Engineering. Acta Biomater **90**, 37, 2019.

51. Trachtenberg, J.E., Placone, J.K., Smith, B.T., Fisher, J.P., and Mikos, A.G. Extrusion-Based 3d Printing of Poly(Propylene Fumarate) Scaffolds with Hydroxyapatite Gradients. J Biomater Sci Polym Ed **28**, 532, 2017.

Downloaded by Ucsf Library University of California San Francisco from www.liebertpub.com at 11/08/19. For personal use only.

Tissue Engineering
Multi-Material Dual Gradient 3D Printing for Osteogenic Differentiation and Spatial Segregation (DOI: 10.1089/ten.TEA.2019.0204)
This paper has been peer-reviewed and accepted for publication, but has yet to undergo copyediting and proof correction. The final published version may differ from this proof.

52. Lam, J., Lu, S., Meretoja, V.V., Tabata, Y., Mikos, A.G., and Kasper, F.K. Generation of Osteochondral Tissue Constructs with Chondrogenically and Osteogenically Predifferentiated Mesenchymal Stem Cells Encapsulated in Bilayered Hydrogels. Acta Biomater **10**, 1112, 2014.

53. Dominici, M., Le Blanc, K., Mueller, I., Slaper-Cortenbach, I., Marini, F., Krause, D., Deans, R., Keating, A., Prockop, D., and Horwitz, E. Minimal Criteria for Defining Multipotent Mesenchymal Stromal Cells. The International Society for Cellular Therapy Position Statement. Cytotherapy **8**, 315, 2006.

54. Bancroft, G.N., Sikavitsas, V.I., van den Dolder, J., Sheffield, T.L., Ambrose, C.G., Jansen, J.A., and Mikos, A.G. Fluid Flow Increases Mineralized Matrix Deposition in 3d Perfusion Culture of Marrow Stromal Osteoblasts in a Dose-Dependent Manner. Proc Natl Acad Sci **99**, 12600, 2002.

55. Lu, S., Lee, E.J., Lam, J., Tabata, Y., and Mikos, A.G. Evaluation of Gelatin Microparticles as Adherent-Substrates for Mesenchymal Stem Cells in a Hydrogel Composite. Ann Biomed Eng **44**, 1894, 2016.

56. Du, Y., Liu, H., Yang, Q., Wang, S., Wang, J., Ma, J., Noh, I., Mikos, A.G., and Zhang, S. Selective Laser Sintering Scaffold with Hierarchical Architecture and Gradient Composition for Osteochondral Repair in Rabbits. Biomaterials **137**, 37, 2017.

57. Huang, W., Carlsen, B., Wulur, I., Rudkin, G., Ishida, K., Wu, B., Yamaguchi, D.T., and Miller, T.A. Bmp-2 Exerts Differential Effects on Differentiation of Rabbit Bone Marrow Stromal Cells Grown in Two-Dimensional and Three-Dimensional Systems and Is Required for in Vitro Bone Formation in a Plga Scaffold. Exp Cell Res **299**, 325, 2004.

58. Smoak, M.M., Han, A., Watson, E., Kishan, A., Grande-Allen, K.J., Cosgriff-Hernandez, E., and Mikos, A.G. Fabrication and Characterization of Electrospun Decellularized Muscle-Derived Scaffolds. Tissue Eng Part C Methods **25**, 276, 2019.

Downloaded by Ucsf Library University of California San Francisco from www.liebertpub.com at 11/08/19. For personal use only.

Tissue Engineering
Multi-Material Dual Gradient 3D Printing for Osteogenic Differentiation and Spatial Segregation (DOI: 10.1089/ten.TEA.2019.0204)
This paper has been peer-reviewed and accepted for publication, but has yet to undergo copyediting and proof correction. The final published version may differ from this proof.

59. Sikavitsas, V.I., Bancroft, G.N., Holtorf, H.L., Jansen, J.A., and Mikos, A.G. Mineralized Matrix Deposition by Marrow Stromal Osteoblasts in 3d Perfusion Culture Increases with Increasing Fluid Shear Forces. Proc Natl Acad Sci U S A **100**, 14683, 2003.

60. Lian, J.B., and Stein, G.S. Concepts of Osteoblast Growth and Differentiation: Basis for Modulation of Bone Cell Development and Tissue Formation. Crit Rev Oral Biol Med **3**, 269, 1992.

61. Lian, J.B., and Stein, G.S. Development of the Osteoblast Phenotype: Molecular Mechanisms Mediating Osteoblast Growth and Differentiation. Iowa Orthop J **15**, 118, 1995.

62. Takahashi, Y., Yamamoto, M., and Tabata, Y. Osteogenic Differentiation of Mesenchymal Stem Cells in Biodegradable Sponges Composed of Gelatin and Beta-Tricalcium Phosphate. Biomaterials **26**, 3587, 2005.

63. Diaz-Gomez, L., Kontoyiannis, P.D., Melchiorri, A.J., and Mikos, A.G. Three-Dimensional Printing of Tissue Engineering Scaffolds with Horizontal Pore and Composition Gradients. Tissue Eng Part C Methods **25**, 411, 2019.

64. Smoak, M., Hogan, K., Kriegh, L., Chen, C., Terrell, L.B., Qureshi, A.T., Monroe, W.T., Gimble, J.M., and Hayes, D.J. Modulation of Mesenchymal Stem Cell Behavior by Nano-and Micro-Sized B-Tricalcium Phosphate Particles in Suspension and Composite Structures. J Nanopart Res **17**, 182, 2015.

65. Marino, G., Rosso, F., Cafiero, G., Tortora, C., Moraci, M., Barbarisi, M., and Barbarisi, A. Beta-Tricalcium Phosphate 3d Scaffold Promote Alone Osteogenic Differentiation of Human Adipose Stem Cells: In Vitro Study. J Mater Sci Mater Med **21**, 353, 2010.

66. Lu, Z., and Zreiqat, H. Beta-Tricalcium Phosphate Exerts Osteoconductivity through Alpha2beta1 Integrin and Down-Stream Mapk/Erk Signaling Pathway. Biochem Biophys Res Commun **394**, 323, 2010.

Downloaded by Ucsf Library University of California San Francisco from www.liebertpub.com at 11/08/19. For personal use only.

Tissue Engineering
Multi-Material Dual Gradient 3D Printing for Osteogenic Differentiation and Spatial Segregation (DOI: 10.1089/ten.TEA.2019.0204)
This paper has been peer-reviewed and accepted for publication, but has yet to undergo copyediting and proof correction. The final published version may differ from this proof.

67. Wen, L., Wang, Y., Wang, H., Kong, L., Zhang, L., Chen, X., and Ding, Y. L-Type Calcium Channels Play a Crucial Role in the Proliferation and Osteogenic Differentiation of Bone Marrow Mesenchymal Stem Cells. Biochem Biophys Res Commun **424**, 439, 2012.

68. Aquino-Martínez, R., Artigas, N., Gámez, B., Rosa, J.L., and Ventura, F. Extracellular Calcium Promotes Bone Formation from Bone Marrow Mesenchymal Stem Cells by Amplifying the Effects of Bmp-2 on Smad Signalling. PLoS One **12**, e0178158, 2017.

69. Surmenev, R.A., Surmeneva, M.A., and Ivanova, A.A. Significance of Calcium Phosphate Coatings for the Enhancement of New Bone Osteogenesis – a Review. Acta Biomater **10**, 557, 2014.

70. dos Santos, E.A., Farina, M., Soares, G.A., and Anselme, K. Chemical and Topographical Influence of Hydroxyapatite and B-Tricalcium Phosphate Surfaces on Human Osteoblastic Cell Behavior. J Biomed Mater Res A **89A**, 510, 2009.

71. Barradas, A.M.C., Fernandes, H.A.M., Groen, N., Chai, Y.C., Schrooten, J., van de Peppel, J., van Leeuwen, J.P.T.M., van Blitterswijk, C.A., and de Boer, J. A Calcium-Induced Signaling Cascade Leading to Osteogenic Differentiation of Human Bone Marrow-Derived Mesenchymal Stromal Cells. Biomaterials **33**, 3205, 2012.

72. Heo, S.J., Kim, S.E., Wei, J., Hyun, Y.T., Yun, H.S., Kim, D.H., Shin, J.W., and Shin, J.W. Fabrication and Characterization of Novel Nano-and Micro-Ha/Pcl Composite Scaffolds Using a Modified Rapid Prototyping Process. J Biomed Mater Res A **89**, 108, 2009.

73. Williams, J.M., Adewunmi, A., Schek, R.M., Flanagan, C.L., Krebsbach, P.H., Feinberg, S.E., Hollister, S.J., and Das, S. Bone Tissue Engineering Using Polycaprolactone Scaffolds Fabricated Via Selective Laser Sintering. Biomaterials **26**, 4817, 2005.

74. Park, S.A., Lee, S.H., and Kim, W.D. Fabrication of Porous Polycaprolactone/Hydroxyapatite (Pcl/Ha) Blend Scaffolds Using a 3d Plotting System for Bone Tissue Engineering. Bioprocess Biosyst Eng **34**, 505, 2011.

Downloaded by Ucsf Library University of California San Francisco from www.liebertpub.com at 11/08/19. For personal use only.

Tissue Engineering
Multi-Material Dual Gradient 3D Printing for Osteogenic Differentiation and Spatial Segregation (DOI: 10.1089/ten.TEA.2019.0204)
This paper has been peer-reviewed and accepted for publication, but has yet to undergo copyediting and proof correction. The final published version may differ from this proof.

75. Park, J., Lee, S.J., Jo, H.H., Lee, J.H., Kim, W.D., Lee, J.Y., and Su, A. Fabrication and Characterization of 3d-Printed Bone-Like B-Tricalcium Phosphate/Polycaprolactone Scaffolds for Dental Tissue Engineering. J Ind Eng Chem **46**, 175, 2017.

76. Kim, K., Yeatts, A., Dean, D., and Fisher, J.P. Stereolithographic Bone Scaffold Design Parameters: Osteogenic Differentiation and Signal Expression. Tissue Eng Part B Rev **16**, 523, 2010.

77. Huri, P.Y., Ozilgen, B.A., Hutton, D.L., and Grayson, W.L. Scaffold Pore Size Modulates in Vitro Osteogenesis of Human Adipose-Derived Stem/Stromal Cells. Biomed Mater **9**, 045003, 2014.

78. Kasten, P., Beyen, I., Niemeyer, P., Luginbühl, R., Bohner, M., and Richter, W. Porosity and Pore Size of B-Tricalcium Phosphate Scaffold Can Influence Protein Production and Osteogenic Differentiation of Human Mesenchymal Stem Cells: An in Vitro and in Vivo Study. Acta Biomater **4**, 1904, 2008.

79. Kim, K., Dean, D., Wallace, J., Breithaupt, R., Mikos, A.G., and Fisher, J.P. The Influence of Stereolithographic Scaffold Architecture and Composition on Osteogenic Signal Expression with Rat Bone Marrow Stromal Cells. Biomaterials **32**, 3750, 2011.

80. Kim, K., Dean, D., Wallace, J., Breithaupt, R., Mikos, A.G., and Fisher, J.P. The Influence of Stereolithographic Scaffold Architecture and Composition on Osteogenic Signal Expression with Rat Bone Marrow Stromal Cells. Biomaterials **32**, 3750, 2011.

81. Matsiko, A., Gleeson, J.P., and O'Brien, F.J. Scaffold Mean Pore Size Influences Mesenchymal Stem Cell Chondrogenic Differentiation and Matrix Deposition. Tissue Eng Part A **21**, 486, 2014.

82. Harris, G.M., Piroli, M.E., and Jabbarzadeh, E. Deconstructing the Effects of Matrix Elasticity and Geometry in Mesenchymal Stem Cell Lineage Commitment. Adv Funct Mater **24**, 2396, 2014.

Downloaded by Ucsf Library University of California San Francisco from www.liebertpub.com at 11/08/19. For personal use only.

Tissue Engineering
Multi-Material Dual Gradient 3D Printing for Osteogenic Differentiation and Spatial Segregation (DOI: 10.1089/ten.TEA.2019.0204)
This paper has been peer-reviewed and accepted for publication, but has yet to undergo copyediting and proof correction. The final published version may differ from this proof.

83. McMurtrey, R.J. Roles of Diffusion Dynamics in Stem Cell Signaling and Three-Dimensional Tissue Development. Stem Cells Dev **26**, 1293, 2017.

84. Rabe, M., Verdes, D., and Seeger, S. Understanding Protein Adsorption Phenomena at Solid Surfaces. Adv Colloid Interface Sci **162**, 87, 2011.

85. Kretlow, J.D., and Mikos, A.G. Review: Mineralization of Synthetic Polymer Scaffolds for Bone Tissue Engineering. Tissue Engineering **13**, 927, 2007.

86. Karageorgiou, V., and Kaplan, D. Porosity of 3d Biomaterial Scaffolds and Osteogenesis. Biomaterials **26**, 5474, 2005.

87. Stein, G.S., Lian, J.B., and Owen, T.A. Relationship of Cell Growth to the Regulation of Tissue-Specific Gene Expression During Osteoblast Differentiation. The FASEB Journal **4**, 3111, 1990.

88. Zhu, L., and Skoultchi, A.I. Coordinating Cell Proliferation and Differentiation. Curr Opin Genet Dev **11**, 91, 2001.

Downloaded by Ucsf Library University of California San Francisco from www.liebertpub.com at 11/08/19. For personal use only.

Tissue Engineering
Multi-Material Dual Gradient 3D Printing for Osteogenic Differentiation and Spatial Segregation (DOI: 10.1089/ten.TEA.2019.0204)
This paper has been peer-reviewed and accepted for publication, but has yet to undergo copyediting and proof correction. The final published version may differ from this proof.

Table 1. β-TCP/HA/PCL formulations for 3D printed constructs*.

Formulation	HA (wt%)	β-TCP (wt%)	Pore Gradient
$Pore_U$	10	0	Uniform (M)
$Pore_G$	10	0	Gradient (S,M,L)
$TCP10Pore_U$	10	10	Uniform (M)
$TCP10Pore_G$	10	10	Gradient (S,M,L)
TCP_GPore_U	10	Gradient (0, 10, 20)	Uniform (M)
TCP_GPore_G	10	Gradient (0, 10, 20)	Gradient (S,M,L)
TCP_GPore_{GI}	10	Gradient (0, 10, 20)	Gradient (L,M,S)

*Constructs were fabricated with three distinct fiber spacings: 0.2 mm (small, S), 0.6 mm (medium, M), and 1.0 mm (large, L). Porosity and gradient ceramic concentrations are listed in the orientation, from top to bottom, during cell culture.

Downloaded by Ucsf Library University of California San Francisco from www.liebertpub.com at 11/08/19. For personal use only.

Tissue Engineering
Multi-Material Dual Gradient 3D Printing for Osteogenic Differentiation and Spatial Segregation (DOI: 10.1089/ten.TEA.2019.0204)
This paper has been peer-reviewed and accepted for publication, but has yet to undergo copyediting and proof correction. The final published version may differ from this proof.

Table 2. List of scaffold printing conditions/parameters.

Material	Temperature (°C)	Pressure (bar)	Speed (mm/s)	Pre-Flow (s)	Post-Flow (s)
0 wt% β-TCP 10 wt% HA	160	5.2	1.1	0.85	0.55
10 wt% β-TCP 10 wt% HA	160	6.0	1.3	0.7	0.45
20 wt% β-TCP 10 wt% HA	160	6.2	0.7	0.8	0.7

Downloaded by Ucsf Library University of California San Francisco from www.liebertpub.com at 11/08/19. For personal use only.

Tissue Engineering
Multi-Material Dual Gradient 3D Printing for Osteogenic Differentiation and Spatial Segregation (DOI: 10.1089/ten.TEA.2019.0204)
This paper has been peer-reviewed and accepted for publication, but has yet to undergo copyediting and proof correction. The final published version may differ from this proof.

Table 3. Primer sequences for RT-PCR.

Gene	Forward Primer (5'-3')	Reverse Primer (5'-3')
GAPDH	TCACCATCTTCCAGGAGCGA	CACAATGCCGAAGTGGTCGT
Osteocalcin	CAAAGCCCAGCGGTGCAGAGTCT	AGCTCCCTGCCCGTCGATCAGTT
Osteopontin	CACCATGAGAATCGCCGT	CGTGACTTTGGGTTTCTACGC
Runx2	CCTTCCACTCTCAGTAAGAAGA	TAAGTAAAGGTGGCTGGATAGT

Downloaded by Ucsf Library University of California San Francisco from www.liebertpub.com at 11/08/19. For personal use only.

Tissue Engineering
Multi-Material Dual Gradient 3D Printing for Osteogenic Differentiation and Spatial Segregation (DOI: 10.1089/ten.TEA.2019.0204)
This paper has been peer-reviewed and accepted for publication, but has yet to undergo copyediting and proof correction. The final published version may differ from this proof.

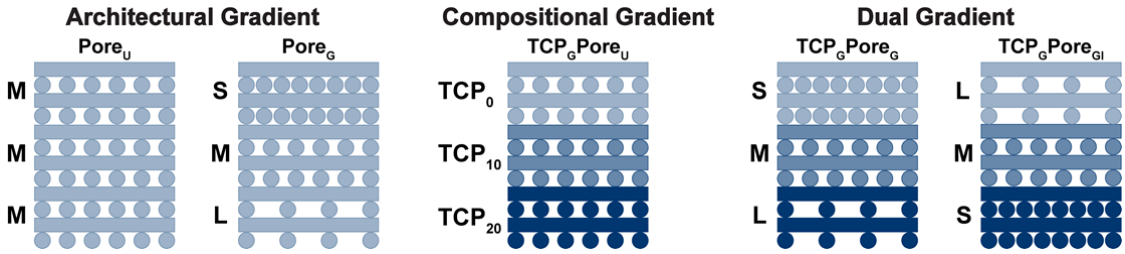

Figure 1. Cross-sectional view of architectural, compositional, and dual gradient constructs presented in the same orientation that was maintained over the duration of the study (the section that was resting on the bottom of the well-plate corresponds to the section at the bottom of the figure). Each construct was comprised of 3 sections that had a fiber spacing of 0.2 mm (S), 0.6 mm (M), or 1.0 mm (L) and a concentration of β-TCP of 0, 10, or 20 wt% as described in Table 1.

Downloaded by Ucsf Library University of California San Francisco from www.liebertpub.com at 11/08/19. For personal use only.

Tissue Engineering
Multi-Material Dual Gradient 3D Printing for Osteogenic Differentiation and Spatial Segregation (DOI: 10.1089/ten.TEA.2019.0204)
This paper has been peer-reviewed and accepted for publication, but has yet to undergo copyediting and proof correction. The final published version may differ from this proof.

Downloaded by Ucsf Library University of California San Francisco from www.liebertpub.com at 11/08/19. For personal use only.

Tissue Engineering
Multi-Material Dual Gradient 3D Printing for Osteogenic Differentiation and Spatial Segregation (DOI: 10.1089/ten.TEA.2019.0204)

This paper has been peer-reviewed and accepted for publication, but has yet to undergo copyediting and proof correction. The final published version may differ from this proof.

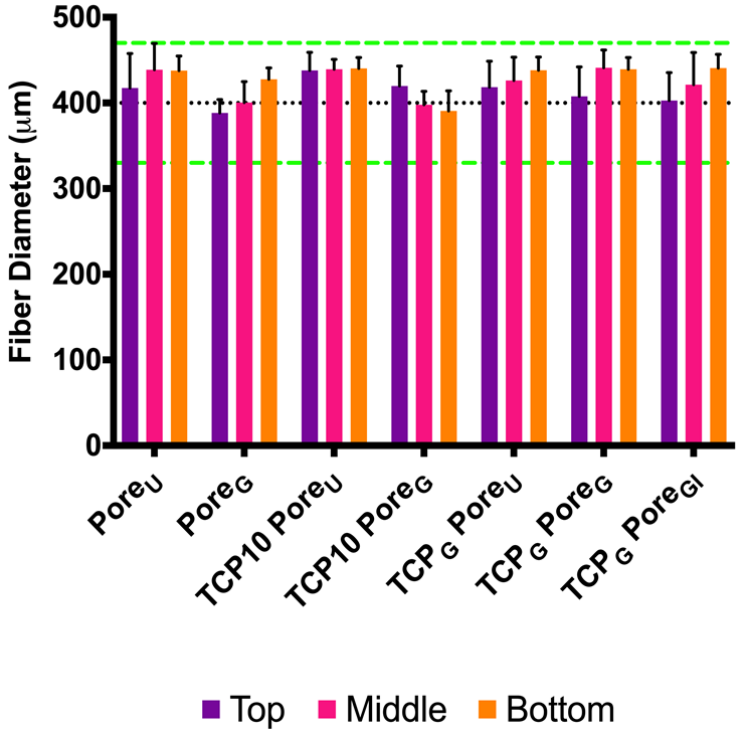

Figure 2. Average fiber diameters within each section of the different formulations investigated (Figure 1). Data are reported as the means ± standard deviation. Top, middle, and bottom refers to the location of the section within the construct during cell culture. Dashed green lines represent 400 ± 60 µm (15% quality control window), while the dashed black line represents the 400 µm desired fiber diameter (n_1=3 scaffolds/group, n_2=3 sections/scaffold, and n_3=10 fibers/section).

Downloaded by Ucsf Library University of California San Francisco from www.liebertpub.com at 11/08/19. For personal use only.

Tissue Engineering
Multi-Material Dual Gradient 3D Printing for Osteogenic Differentiation and Spatial Segregation (DOI: 10.1089/ten.TEA.2019.0204)

This paper has been peer-reviewed and accepted for publication, but has yet to undergo copyediting and proof correction. The final published version may differ from this proof.

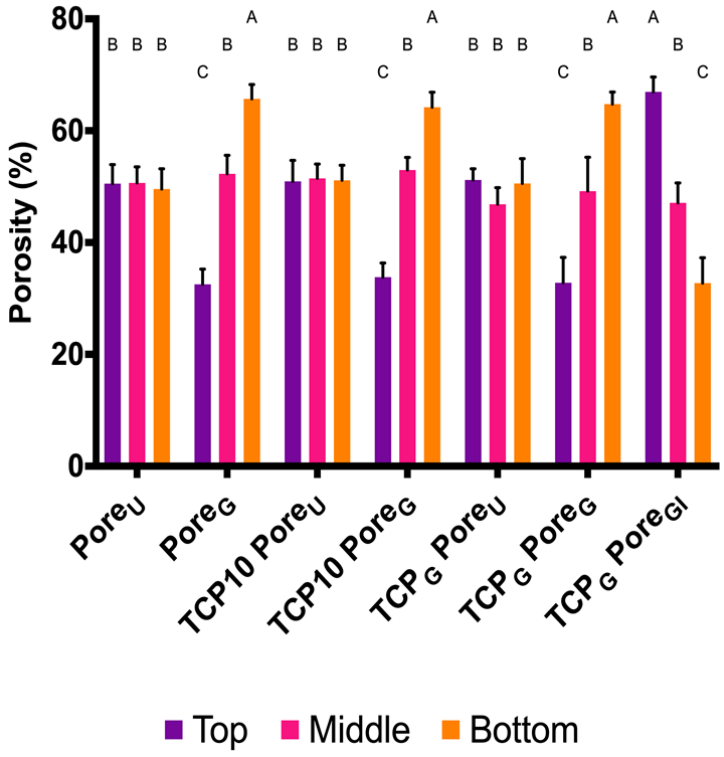

Figure 3. Porosity of the β-TCP/HA/PCL composites (Figure 1) evaluated by μCT. Top, middle, and bottom refers to the location of the section within the construct during cell culture. Data are reported as the means ± standard deviation. Groups that do not share the same letter are significantly different (n=3, $p < 0.05$).

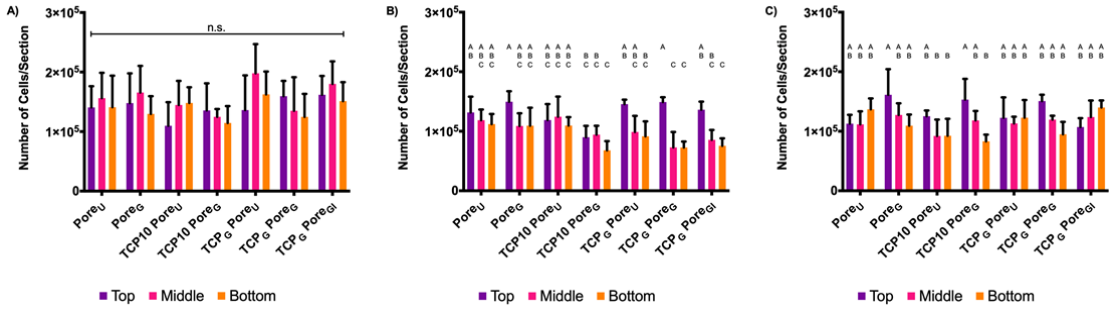

Figure 4. Cellularity of the β-TCP/HA/PCL constructs (Figure 1) at 3 days (A), 14 days (B), and 28 days (C) of culture. Data are reported as the means ± standard deviation. Top, middle, and bottom refers to the location of the section within the construct during cell culture. Within each timepoint, sections that do not share the same letter are significantly different ($p < 0.05$, n=4).

Downloaded by Ucsf Library University of California San Francisco from www.liebertpub.com at 11/08/19. For personal use only.

Tissue Engineering
Multi-Material Dual Gradient 3D Printing for Osteogenic Differentiation and Spatial Segregation (DOI: 10.1089/ten.TEA.2019.0204)
This paper has been peer-reviewed and accepted for publication, but has yet to undergo copyediting and proof correction. The final published version may differ from this proof.

Downloaded by Ucsf Library University of California San Francisco from www.liebertpub.com at 11/08/19. For personal use only.

Tissue Engineering
Multi-Material Dual Gradient 3D Printing for Osteogenic Differentiation and Spatial Segregation (DOI: 10.1089/ten.TEA.2019.0204)

This paper has been peer-reviewed and accepted for publication, but has yet to undergo copyediting and proof correction. The final published version may differ from this proof.

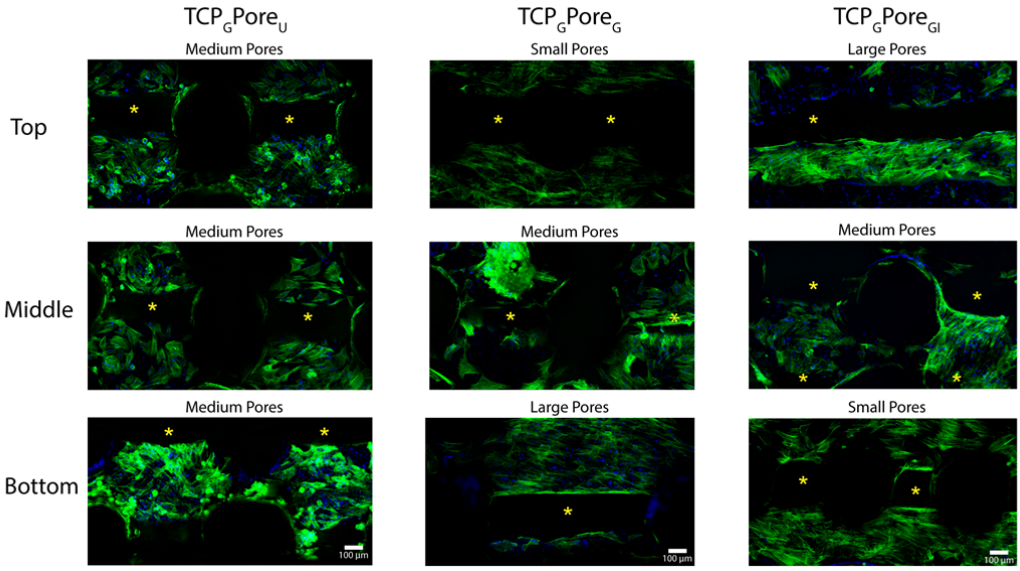

Figure 5. Confocal images of TCP_GPore_U, TCP_GPore_G, and TCP_GPore_{GI}, at day 1. Samples were stained for actin with phalloidin (green) and nuclei with DAPI (blue). Yellow asterisks represent pore spaces within the scaffold. Scale bar is 100 µm.

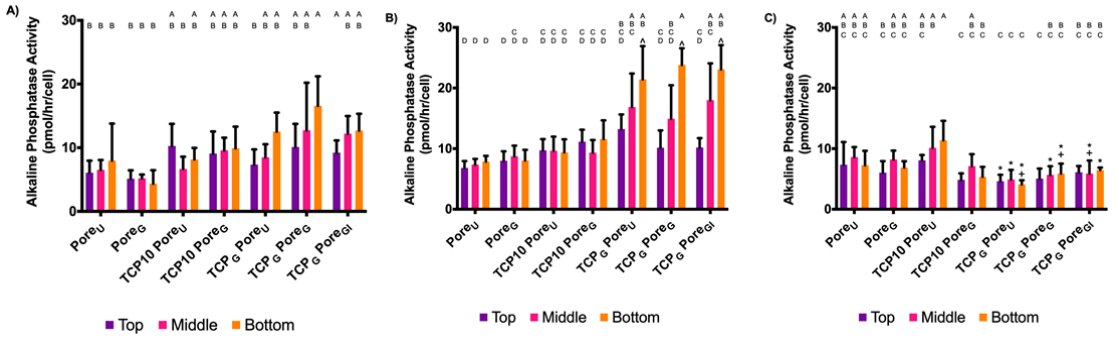

Figure 6. ALP activity of the β-TCP/HA/PCL constructs (Figure 1) at 3 days (A), 14 days (B), and 28 days (C) of culture. Data are reported as the means ± standard deviation. Top, middle, and bottom refers to the location of the section within the construct during cell culture. Within each timepoint, sections that do not share the same letter are significantly different. ^, *, and + indicate significant differences for the same experimental group between 3 and 14, 14 and 28, and 3 and 28 days, respectively ($p < 0.05$, n=4).

Downloaded by Ucsf Library University of California San Francisco from www.liebertpub.com at 11/08/19. For personal use only.

Tissue Engineering
Multi-Material Dual Gradient 3D Printing for Osteogenic Differentiation and Spatial Segregation (DOI: 10.1089/ten.TEA.2019.0204)
This paper has been peer-reviewed and accepted for publication, but has yet to undergo copyediting and proof correction. The final published version may differ from this proof.

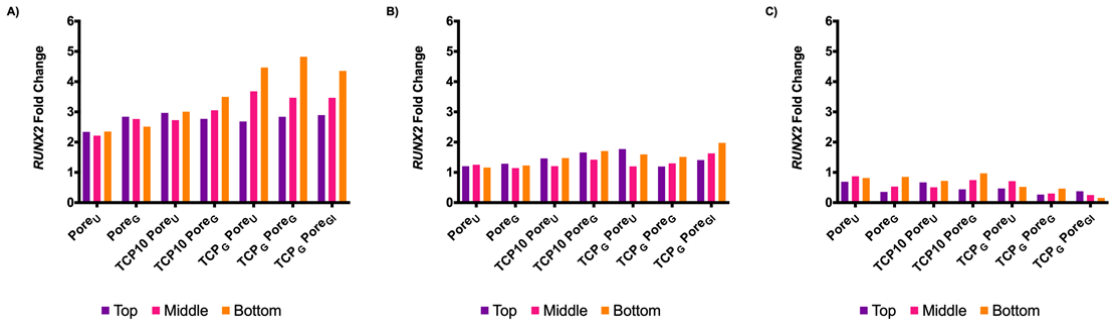

Figure 7. Runx2 fold induction of the β-TCP/HA/PCL constructs (Figure 1) at 3 days (A), 14 days (B), and 28 days (C) of culture. Data are reported as single measurements from four combined sections of similar constructs (n=1). Top, middle, and bottom refers to the location of the section within the construct during cell culture.

Downloaded by Ucsf Library University of California San Francisco from www.liebertpub.com at 11/08/19. For personal use only.

Tissue Engineering
Multi-Material Dual Gradient 3D Printing for Osteogenic Differentiation and Spatial Segregation (DOI: 10.1089/ten.TEA.2019.0204)
This paper has been peer-reviewed and accepted for publication, but has yet to undergo copyediting and proof correction. The final published version may differ from this proof.

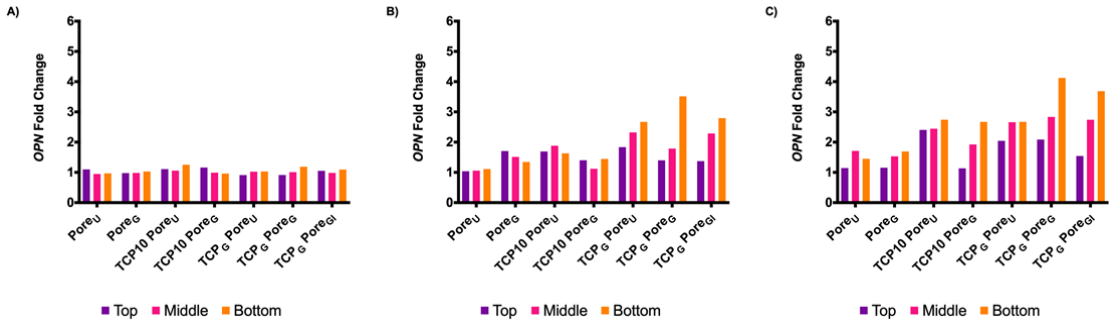

Figure 8. Osteopontin (*Opn*) fold induction of the β-TCP/HA/PCL constructs (Figure 1) at 3 days (A), 14 days (B), and 28 days (C) of culture. Data are reported as single measurements from four combined sections of similar constructs (n=1). Top, middle, and bottom refers to the location of the section within the construct during cell culture.

Downloaded by Ucsf Library University of California San Francisco from www.liebertpub.com at 11/08/19. For personal use only.

Tissue Engineering
Multi-Material Dual Gradient 3D Printing for Osteogenic Differentiation and Spatial Segregation (DOI: 10.1089/ten.TEA.2019.0204)
This paper has been peer-reviewed and accepted for publication, but has yet to undergo copyediting and proof correction. The final published version may differ from this proof.

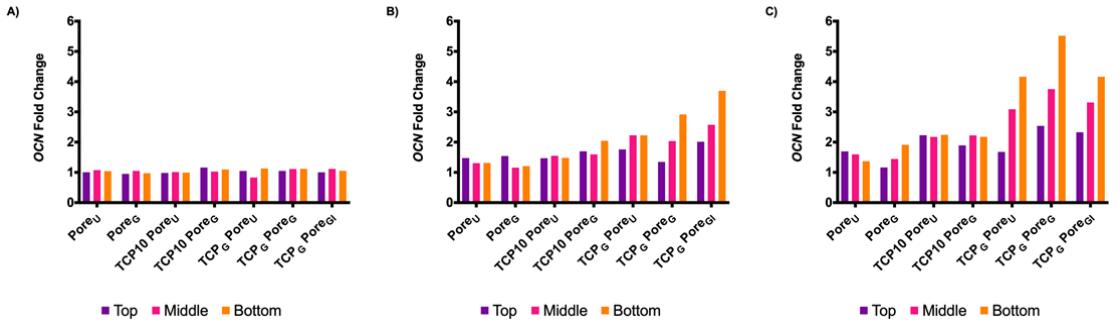

Figure 9. Osteocalcin (*Ocn*) fold induction of the β-TCP/HA/PCL constructs (Figure 1) at 3 days (A), 14 days (B), and 28 days (C) of culture. Data are reported as single measurements from four combined sections of similar constructs (n=1). Top, middle, and bottom refers to the location of the section within the construct during cell culture.

Downloaded by Ucsf Library University of California San Francisco from www.liebertpub.com at 11/08/19. For personal use only.

Tissue Engineering
Multi-Material Dual Gradient 3D Printing for Osteogenic Differentiation and Spatial Segregation (DOI: 10.1089/ten.TEA.2019.0204)
This paper has been peer-reviewed and accepted for publication, but has yet to undergo copyediting and proof correction. The final published version may differ from this proof.

Downloaded by Ucsf Library University of California San Francisco from www.liebertpub.com at 11/08/19. For personal use only.

Tissue Engineering
Multi-Material Dual Gradient 3D Printing for Osteogenic Differentiation and Spatial Segregation (DOI: 10.1089/ten.TEA.2019.0204)

This paper has been peer-reviewed and accepted for publication, but has yet to undergo copyediting and proof correction. The final published version may differ from this proof.

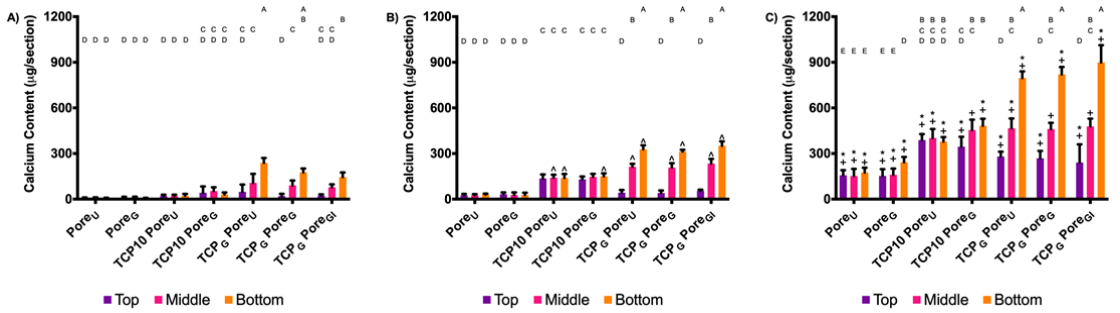

Figure 10. Calcium deposition in the β-TCP/HA/PCL constructs (Figure 1) on a per-section basis at 3 days (A), 14 days (B), and 28 days (C) of culture. Data are reported as the means ± standard deviation. Top, middle, and bottom refers to the location of the section within the construct during cell culture. Within each timepoint, sections that do not share the same letter are significantly different. ^, *, and + indicate significant differences for the same experimental group between 3 and 14, 14 and 28, and 3 and 28 days, respectively ($p < 0.05$, n=4).

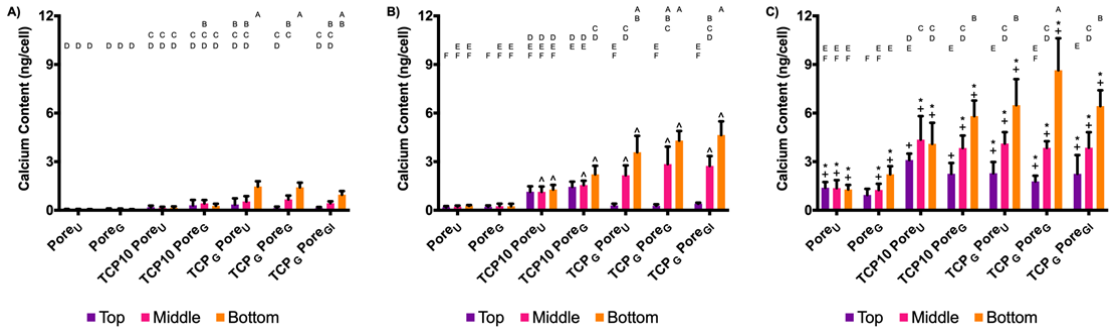

Figure 11. Calcium deposition in the β-TCP/HA/PCL constructs (Figure 1) on a per-cell basis at 3 days (A), 14 days (B), and 28 days (C) of culture. Top, middle, and bottom refers to the location of the section within the construct during cell culture. Data are reported as the means ± standard deviation. Within each timepoint, sections that do not share the same letter are significantly different. ^, *, and + indicate statistical differences for the same experimental group between 3 and 14, 14 and 28, and 3 and 28 days, respectively ($p < 0.05$, n=4).

Downloaded by Ucsf Library University of California San Francisco from www.liebertpub.com at 11/08/19. For personal use only.

Tissue Engineering
Multi-Material Dual Gradient 3D Printing for Osteogenic Differentiation and Spatial Segregation (DOI: 10.1089/ten.TEA.2019.0204)
This paper has been peer-reviewed and accepted for publication, but has yet to undergo copyediting and proof correction. The final published version may differ from this proof.

Downloaded by Ucsf Library University of California San Francisco from www.liebertpub.com at 11/08/19. For personal use only.

Tissue Engineering
Multi-Material Dual Gradient 3D Printing for Osteogenic Differentiation and Spatial Segregation (DOI: 10.1089/ten.TEA.2019.0204)

This paper has been peer-reviewed and accepted for publication, but has yet to undergo copyediting and proof correction. The final published version may differ from this proof.

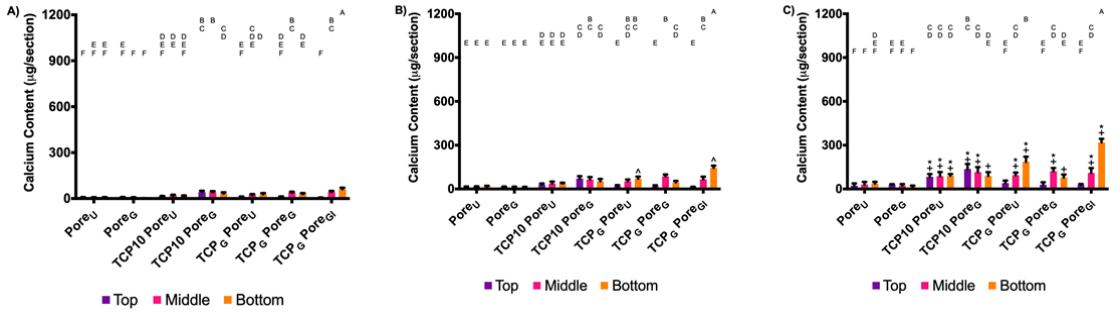

Figure S1. Calcium deposition in the acellular β-TCP/HA/PCL constructs (Figure 1) that were incubated for 3 days (A), 14 days (B), and 28 days (C). Data are reported as the means ± standard deviation. Top, middle, and bottom refers to the location of the section within the construct during incubation. Within each timepoint, sections that do not share the same letter are significantly different. ^, *, and + indicate significant differences for the same experimental group between 3 and 14, 14 and 28, and 3 and 28 days, respectively ($p < 0.05$, n=4).

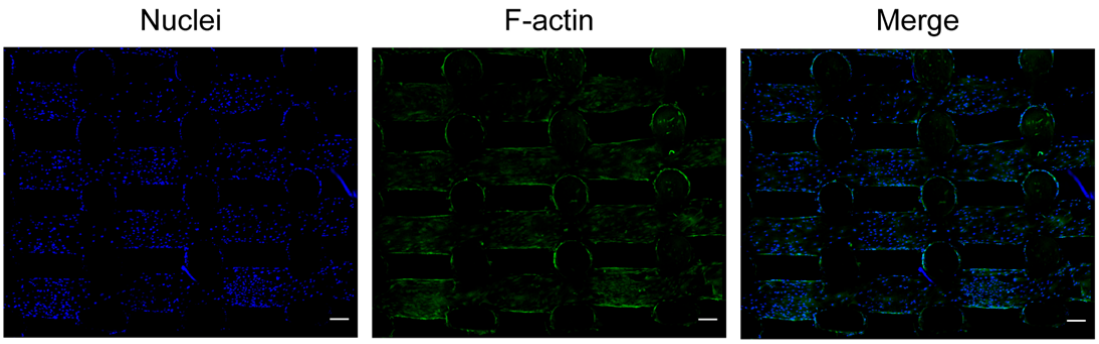

Figure S2. MSC morphology and distribution at 3 days on $Pore_U$ constructs (Figure 1). Constructs were cut longitudinally, and the layer at the bottom of the image was resting on the bottom of the well. Scale bar is 200 µm in all panels.

Downloaded by Ucsf Library University of California San Francisco from www.liebertpub.com at 11/08/19. For personal use only.

Tissue Engineering
Multi-Material Dual Gradient 3D Printing for Osteogenic Differentiation and Spatial Segregation (DOI: 10.1089/ten.TEA.2019.0204)
This paper has been peer-reviewed and accepted for publication, but has yet to undergo copyediting and proof correction. The final published version may differ from this proof.

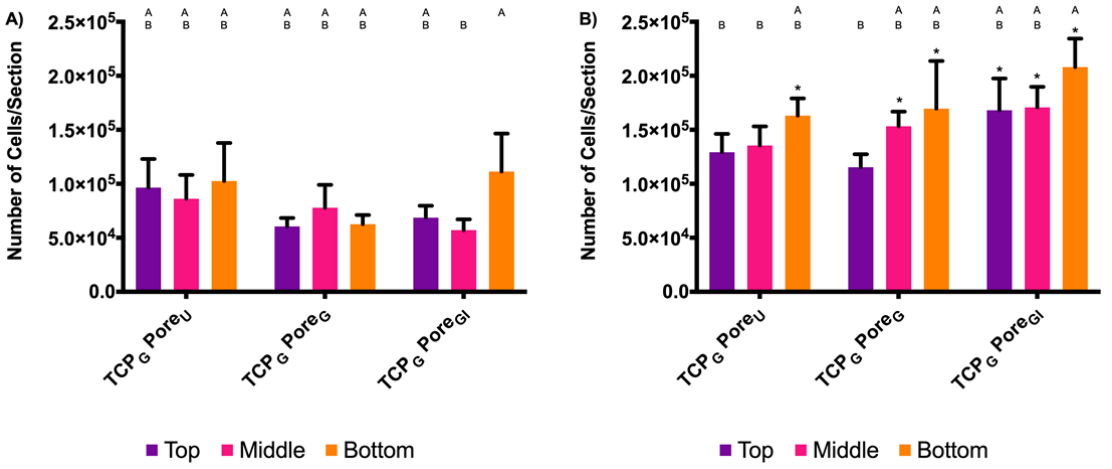

Figure S3. Cellularity of the β-TCP/HA/PCL constructs (Figure 1) at 1 day (A), and 3 days (B) of culture. Data are reported as the means ± standard deviation. Top, middle, and bottom refers to the location of the section within the construct during cell culture. Within each timepoint, sections that do not share the same letter are significantly different. * indicates significant differences for the same experimental group between 1 and 3 days ($p < 0.05$, n=4)

Downloaded by Ucsf Library University of California San Francisco from www.liebertpub.com at 11/08/19. For personal use only.

Tissue Engineering
Multi-Material Dual Gradient 3D Printing for Osteogenic Differentiation and Spatial Segregation (DOI: 10.1089/ten.TEA.2019.0204)
This paper has been peer-reviewed and accepted for publication, but has yet to undergo copyediting and proof correction. The final published version may differ from this proof.

Downloaded by Ucsf Library University of California San Francisco from www.liebertpub.com at 11/08/19. For personal use only.

Tissue Engineering
Multi-Material Dual Gradient 3D Printing for Osteogenic Differentiation and Spatial Segregation (DOI: 10.1089/ten.TEA.2019.0204)
This paper has been peer-reviewed and accepted for publication, but has yet to undergo copyediting and proof correction. The final published version may differ from this proof.

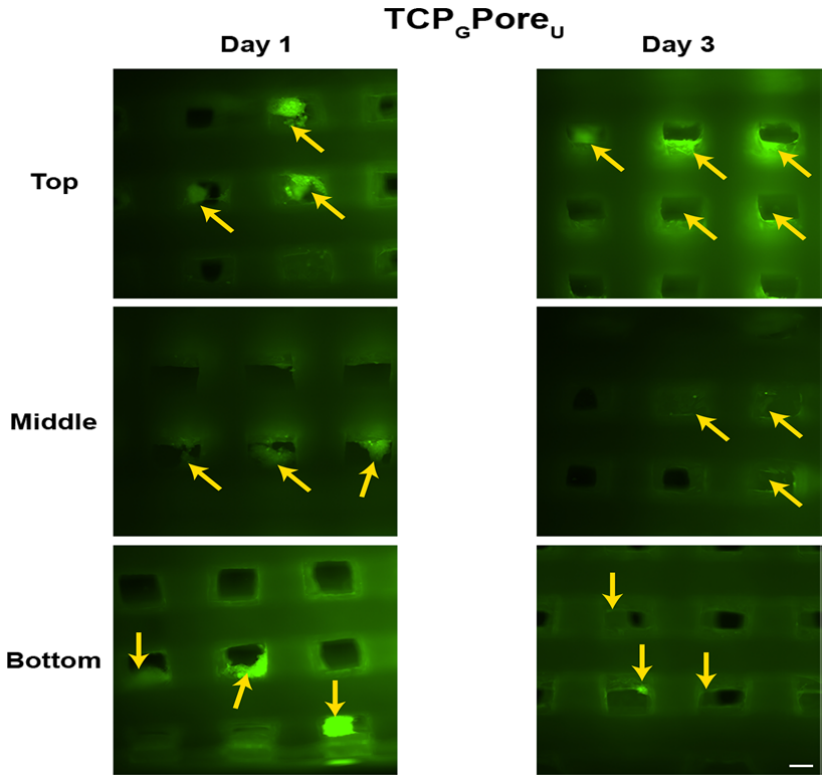

Figure S4. Fluorescence microscopy images of TCP$_G$Pore$_U$ at day 1 and 3. Samples were stained with phalloidin (green) to visualize the actin. Images were taken at different vertical positions within a scaffold (top, middle, or bottom). Yellow arrows denote observed cell aggregates. Scale bar is 200 µm.

Downloaded by Ucsf Library University of California San Francisco from www.liebertpub.com at 11/08/19. For personal use only.

Tissue Engineering
Multi-Material Dual Gradient 3D Printing for Osteogenic Differentiation and Spatial Segregation (DOI: 10.1089/ten.TEA.2019.0204)

This paper has been peer-reviewed and accepted for publication, but has yet to undergo copyediting and proof correction. The final published version may differ from this proof.

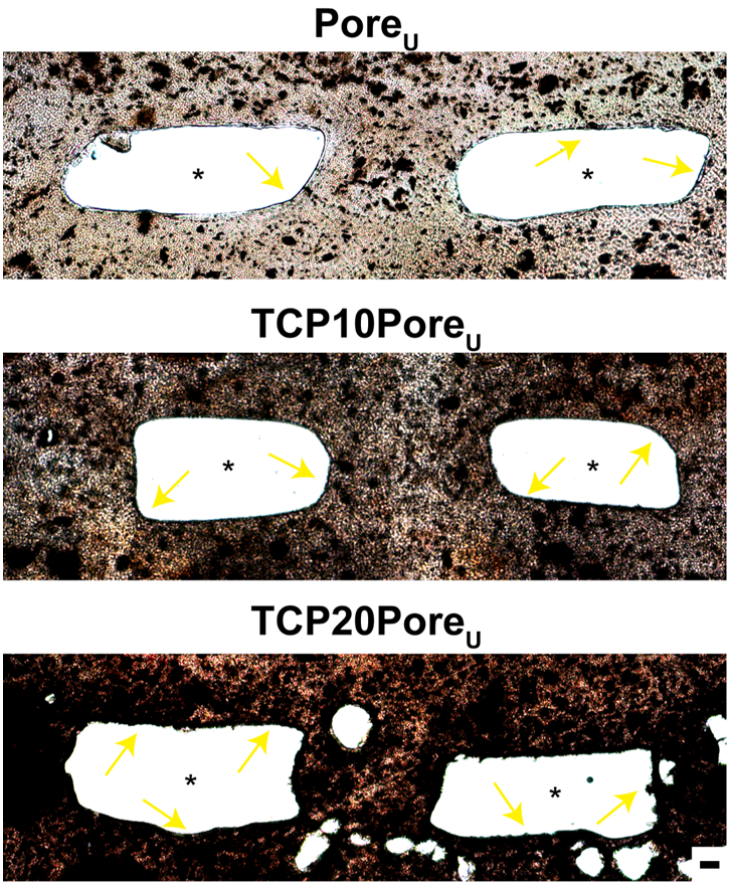

Figure S5. Representative cross-sectional high magnification histological images of medium pore β-TCP/HA/PCL constructs after 28 days of cell seeding. Sections were stained with von Kossa which stains mineral deposits, as well as β-TCP and HA, black. Asterisk denote a pore space. Yellow arrows denote mineralized regions. Scale bar in the lower right represents 100 µm.